Facilitation of axon regeneration by enhancing mitochondrial transport and rescuing energy deficits

Bing Zhou,[1] Panpan Yu,[2] Mei-Yao Lin,[1] Tao Sun,[1] Yanmin Chen,[1] and Zu-Hang Sheng[1]

[1]Synaptic Functions Section, The Porter Neuroscience Research Center, National Institute of Neurological Disorders and Stroke, National Institutes of Health, Bethesda, MD 20892
[2]Guangdong–Hong Kong–Macau Institute of CNS Regeneration, Ministry of Education Joint International Research Laboratory of CNS Regeneration, Jinan University, Guangzhou 510632, China

Although neuronal regeneration is a highly energy-demanding process, axonal mitochondrial transport progressively declines with maturation. Mature neurons typically fail to regenerate after injury, thus raising a fundamental question as to whether mitochondrial transport is necessary to meet enhanced metabolic requirements during regeneration. Here, we reveal that reduced mitochondrial motility and energy deficits in injured axons are intrinsic mechanisms controlling regrowth in mature neurons. Axotomy induces acute mitochondrial depolarization and ATP depletion in injured axons. Thus, mature neuron-associated increases in mitochondria-anchoring protein syntaphilin (SNPH) and decreases in mitochondrial transport cause local energy deficits. Strikingly, enhancing mitochondrial transport via genetic manipulation facilitates regenerative capacity by replenishing healthy mitochondria in injured axons, thereby rescuing energy deficits. An in vivo sciatic nerve crush study further shows that enhanced mitochondrial transport in *snph* knockout mice accelerates axon regeneration. Understanding deficits in mitochondrial trafficking and energy supply in injured axons of mature neurons benefits development of new strategies to stimulate axon regeneration.

Introduction

Mitochondria are cellular power plants that supply ATP essential for neuron growth, survival, and regeneration (Nicholls and Budd, 2000). Because of their extremely varied morphological features, neurons face special challenges to maintain energy homeostasis in distal regions of the axons. Mitochondrial distribution to far distal axons depends on microtubule (MT)-based motors via mechanisms that require ATP hydrolysis (Ruthel and Hollenbeck, 2003; MacAskill and Kittler, 2010; Saxton and Hollenbeck, 2012; Sheng and Cai, 2012). Mitochondria move bidirectionally along axons and frequently change direction. Motile mitochondria can become stationary, and stationary ones can be redistributed in response to changes in metabolic status and growth conditions (Sheng, 2014). In mature axons of the central nervous system (CNS), the majority of mitochondria remain stationary, whereas ~20–30% are motile (Sun et al., 2013). In addition, distal mitochondria need to be removed when their integrity is impaired under certain stress conditions (Miller and Sheetz, 2004; Chang and Reynolds, 2006; Cai et al., 2012).

Although young neurons possess the capacity for robust axon growth during early development, mature CNS axons typically fail to regrow after injury, leading to permanent neurological impairments. Numerous studies in the past have focused on genetic programs, signaling mechanisms, and extracellular inhibitory factors for axon regeneration (see reviews by Schwab and Bartholdi [1996], Case and Tessier-Lavigne [2005], Filbin [2006], Harel and Strittmatter [2006], Yiu and He [2006], Fitch and Silver [2008], Liu et al. [2011], and Cho and Cavalli [2014]). These studies suggest that mature CNS neurons have lost their growth capacity as the result of an intrinsic decline of permissive conditions for regeneration. Thus, it is critical to reveal these intrinsic pathways that account for mature neuron-associated decline of axonal regrowth capacity.

To survive an injury, neurons need to quickly reform an active growth cone where damaged membranes are resealed, cytoskeletal structures are rearranged, and regrowth programs are activated, including synthesis of raw materials, transport, and assembly of axonal components (Bradke et al., 2012). All of these events require high levels of energy consumption. Thus, proper mitochondrial transport into injured axons ensures that metabolically active areas are adequately supplied with ATP. However, two fundamental questions remain to be addressed. (1) Do mature neurons maintain an effective capacity to recruit mitochondria to injured axons? And (2) if this function declines in mature neurons, does enhancing mitochondrial transport enable mature neurons to regain regenerative capacity

---

The Rockefeller University Press $30.00
J. Cell Biol. Vol. 214 No. 1   103–119
www.jcb.org/cgi/doi/10.1083/jcb.201605101

JCB   103

THE JOURNAL OF CELL BIOLOGY

by facilitating the removal of damaged mitochondria from and replenishing healthy ones to injured axons?

Our previous study demonstrated that syntaphilin (SNPH) acts as a "static anchor" specific for axonal mitochondria (Kang et al., 2008; Chen and Sheng, 2013). Deleting murine *snph* results in a substantially increased percentage (∼70%) of motile axonal mitochondria. Conversely, overexpressing SNPH abolishes axonal mitochondrial transport. Most interestingly, SNPH is strictly developmentally regulated in the brain: its expression is hardly detectable in embryonic stages, very low before postnatal day 7 (P7), and peaks at adult stages (Das et al., 2003). The unique pattern of SNPH expression in the brain and its specific role in anchoring axonal mitochondria allow us to propose an attractive hypothesis: mature neuron-associated decline of mitochondrial transport is an intrinsic mechanism controlling axon regrowth capacity. Thus, *snph* knockout (KO) mice provide an ideal model to investigate how mitochondrial trafficking and anchoring influences axonal regenerative capacity.

In the current study, we reveal that enhancing axonal mitochondrial transport in *snph* KO mice facilitates axon regenerative capacity. We further show that axon injury is an acute stress signal that depolarizes mitochondria in the vicinity of the injured site. Enhancing transport helps remove those dysfunctional mitochondria from and replenish healthy ones to the injured axons, thus rescuing energy deficits and facilitating axonal regrowth. Therefore, our study suggests a new cellular target for stimulating axon regeneration and perhaps functional recovery after nerve injury and disease.

Results

Enhanced axon regrowth in *snph* KO cortical neurons

Our previous study identified SNPH as an axonal mitochondrial anchoring protein; deleting *snph* results in a majority (∼70%) of motile axonal mitochondria in cultured hippocampal and cortical neurons (Kang et al., 2008; Chen and Sheng, 2013). To examine the in vivo effect of SNPH on axonal mitochondrial transport, we crossed *snph* KO mice with Thy1-Mito-CFP transgenic mice, where mitochondria are labeled with CFP in a subset of neurons (Misgeld et al., 2007). Relative mitochondrial motility was assessed from acute nerve explants after rapid dissection in adult wild-type (WT) and *snph* KO littermates (2 mo old). The crossed *snph*−/−/Mito-CFP mice display robustly enhanced mitochondrial motility along axonal bundles of the sciatic nerve (71.58 ± 2.72%, mean ± standard error, P < 0.0001, Mann–Whitney *U* test) relative to that in control Mito-CFP mice (30.95 ± 2.17%, *n* = 23 images for each genotype from five paired littermates; Videos 1 and 2). This ex vivo imaging further verifies that SNPH acts as an anchoring protein that controls axonal mitochondrial transport. Thus, *snph* KO mice serve as an ideal genetic model for our investigations as to how enhanced transport of axonal mitochondria in mature neurons influences axonal regrowth and regenerative capacity.

We first asked whether enhanced mitochondrial transport in *snph* KO cortical neurons facilitates axon regrowth after axotomy. To address this issue, we applied microfluidic culture devices as we previously described (Zhou et al., 2012), in which neuronal cell bodies and dendrites are restricted to the soma chamber while axons grow into the axon terminal chamber through long (450 µm in length) microgrooves. Neurons at 4 d in

vitro (DIV4) were stained with βIII-tubulin, which labels axons (Fig. 1 A). Deleting *snph* in cortical neurons did not change axonal growth during the early stages of development (DIV5; P = 0.38, *n* = 62) when compared with WT neurons (*n* = 60; Fig. S1, A and B). However, when axons in the terminal chamber were removed by vacuum aspiration (axotomy; Fig. 1 B), we found that *snph* KO neurons display enhanced regrowth capacity 3 d after axotomy (Fig. 1, C–E). Axon regrowth begins as early as 7 h after injury and enters a rapid growth phase by 28 h (Fig. 1, F and G). Regrown axonal areas are significantly increased at 28 h in *snph* KO neurons relative to WT control (P < 0.001). We costained terminal axons with phalloidin to label active growth cones 14 h after axotomy. Deleting *snph* significantly facilitates formation of new growth cones (69.11 ± 2.90%, P = 0.0002) compared with WT neurons (44.46 ± 1.92%; Fig. 1, H and I). Live imaging shows that regenerating axons are mainly grown from the injured tips (Fig. S1 C). Thus, enhancing mitochondrial transport by deleting the *snph* gene facilitates axon regrowth after injury.

Mature neuron-associated decline of mitochondrial transport contributes to failed regrowth

We asked whether SNPH expression contributes to a reduced regrowth capacity in mature CNS neurons. WT cortical neurons in microfluidic devices were axotomized at DIV4 or DIV12 and stained with βIII-tubulin 3 or 6 d after axotomy. Although neurons at DIV7 maintain some regrowth capacity, mature neurons at DIV18 display little axon regrowth (Fig. 2, A–C). A possible mechanism underlying such a striking difference in regrowth capacity between young and mature neurons may be caused by development-dependent cellular pathways. To address this issue, we examined the relative expression of SNPH and other mitochondrial proteins in various developmental stages of cultured neurons between DIV3 and DIV22, mouse brains at embryonic day (E) 18 and adult. To our surprise, mature neuron-associated decline of regrowth capacity correlates with progressively increased SNPH expression: its expression is hardly detectable in E18 brains and in cultured neurons before DIV3, readily detected after DIV9, and peaks at DIV22 in culture (Fig. 2, D and E), an expression pattern consistent with our previous findings from rat brains (Das et al., 2003). There were no other proteins detected showing such changes, including kinesin-1 (KIF5), kinesin adaptors Trak2 and Miro1/2, dynein intermediate chain (DIC), and outer mitochondrial membrane proteins TOM20 and VDAC. Furthermore, there is no significant change (P = 0.25) in Miro1/2 expression in WT and *snph* KO cortical neurons at DIV14 (Fig. S1 D). In addition, we expressed HA-SNPH or HA control in cortical neurons and detected no observable change in Miro1/2 expression at DIV14 (P = 0.16; Fig. S1 E).

The unique expression pattern suggests that SNPH controls mitochondrial transport in mature neurons. Consistent with this hypothesis, axonal mitochondria display progressively reduced motility from DIV7 to DIV18 (Fig. 2, F and G). The relative axonal mitochondrial motility at DIV7 is 47.60 ± 4.60%, two times higher than that at DIV18 (22.88 ± 3.09%, P < 0.001). To exclude a general transport decline caused by the long-term neuronal culture, we examined the axonal transport of late endosomes as an internal control and found no decline during the same maturation stages (Fig. 2, F and H). These results suggest that elevated SNPH expression in mature neurons is one of the intrinsic mechanisms diminishing axonal regenerative capacity.
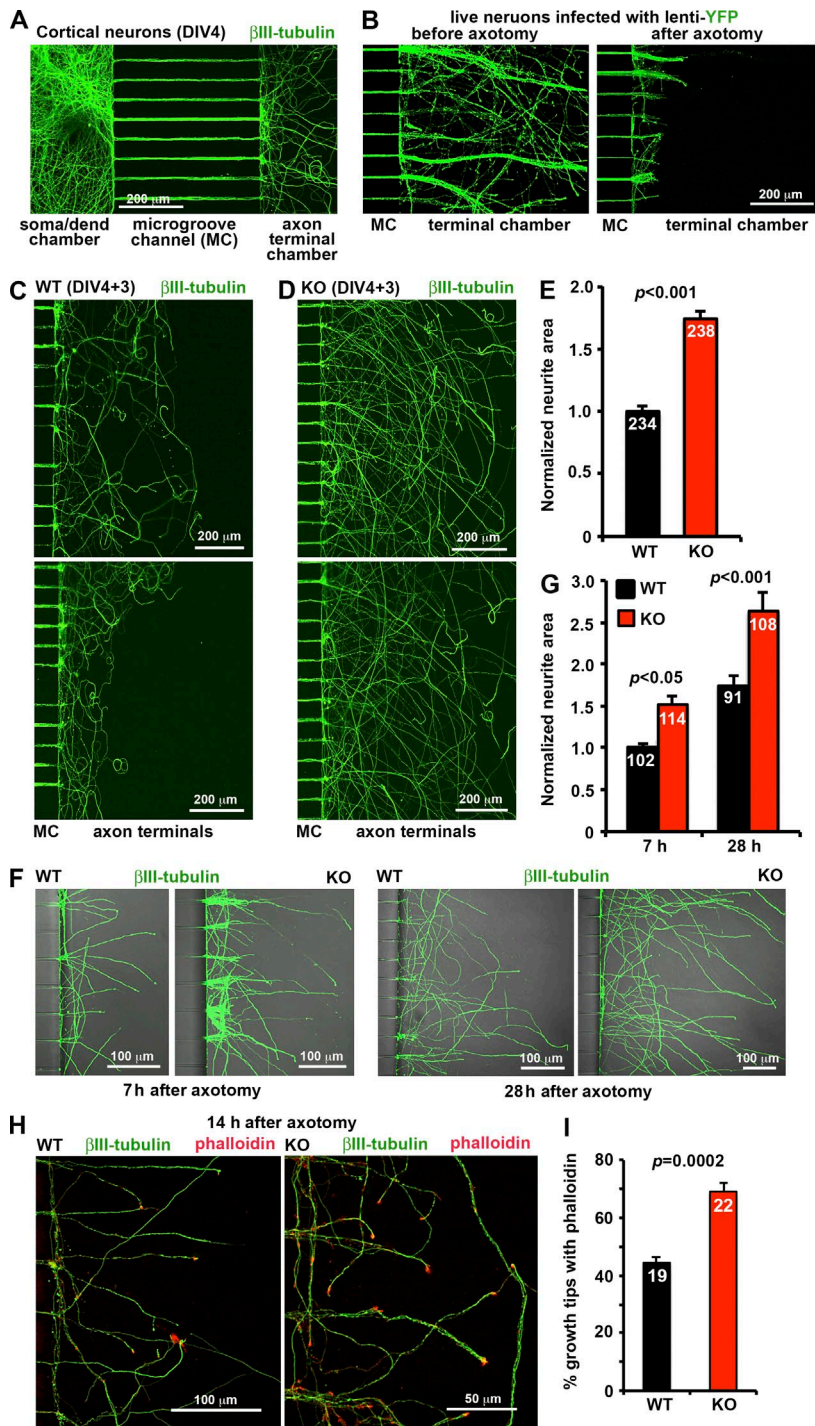
Figure 1. ***snph* KO cortical neurons display enhanced axon regrowth capacity.** (A and B) A microfluidic chamber allows physical and fluidic separation of axons from cell bodies and dendrites. Cortical neurons were seeded in the soma chamber where cell bodies and dendrites are restricted to the soma chamber, whereas axons grow into the axon terminal chamber through the microgroove channels (MC; 450 µm in length). The device (a) allows quick and definitive detection of axons, (b) determines axon directionality, (c) reduces background signals from glial and neuronal cell bodies and dendrites, (d) permits axotomy along the edge of microgrooves by vacuum aspiration, and (e) measures axon regrowth. Neurons were stained with βIII-tubulin (A) or infected with lenti-YFP (B); axon removal in the terminal chamber by vacuum aspiration was confirmed by imaging live neurons expressing YFP before and after axotomy (B). (C–E) Images (C and D) and quantitative analysis (E) showing enhanced axon regrowth after axotomy in *snph* KO neurons. WT (C) and *snph* KO (D) cortical neurons were axotomized at DIV4 and allowed to regrow for 3 d. Axons were immunostained with βIII-tubulin at DIV7. Note that the normalized area of regenerating axons was significantly increased in *snph* KO neurons relative to controls (P < 0.001). (F and G) Images (F) and quantitative analysis (G) of WT and *snph* KO cortical neurons showing early phases of axon regrowth at 7 and 28 h after axotomy. (H and I) Representative images (H) and quantitative analysis (I) showing the formation of new growth cones after axotomy. Axonal terminals were costained with βIII-tubulin and Alexa Fluor 543 phalloidin 14 h after axotomy. Note that deleting *snph* facilitates the formation of growth cones (69.11 ± 2.90%, P = 0.0002) compared with WT (44.46 ± 1.92%) from injured axon tips. Imaging data were pooled from a total number of microgroove channels indicated within bars (E and G) taken from three pairs of littermates or a total number of axonal terminal chambers indicated within bars (I) and expressed as mean ± SE (Student's *t* test).

Mature neurons regain regrowth capacity by enhancing mitochondrial transport

Mature neurons at DIV18 lose their regrowth capacity after axotomy (Fig. 2, A–C) and display a substantial decline in axonal mitochondrial transport (Fig. 2, F–H), raising a question as to whether mature neurons can regain their regrowth capacity by enhancing mitochondrial transport. To address this issue, we manipulated axonal mitochondrial motility in cortical neurons by coexpressing DsRed-Mito with SNPH, SNPH-dMTB, an SNPH loss-of-function mutant deleting its anchoring domain (Kang et al., 2008), or Miro1 via lentivirus infection. Cultured neurons display strikingly different motility patterns of mito-chondria along the microgrooves after transgene expression (Fig. 3 A). Expressing SNPH abolishes axonal mitochondrial motility, whereas expressing Miro1 enhances their bidirectional transport along the microgrooves relative to control neurons (Fig. 3 B and Videos 3–5). To assess axon regrowth after axotomy, these cortical neurons were coinfected with Lenti-GFP to visualize axons in the terminal chambers and grown for 12 d before axotomy. Axonal regrowth was evaluated 6 d after injury (DIV18). Although neurons coexpressing SNPH show very limited axon regrowth, enhancing mitochondrial transport by expressing Miro1 robustly increases axon regrowth capacity when compared with neurons expressing SNPH-dMTB (Fig. 3, C and
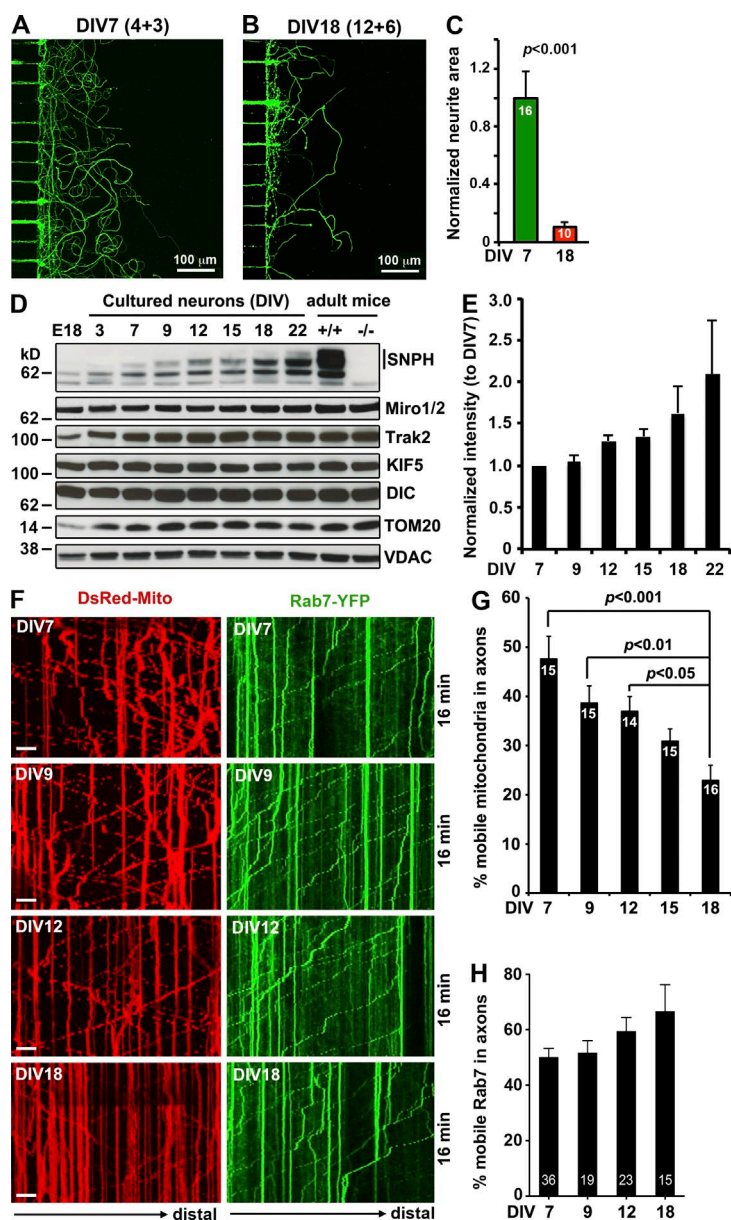
A DIV7 (4+3)   **B** DIV18 (12+6)   **C**

100 μm   100 μm

Figure 2. **SNPH-mediated mitochondrial anchoring contributes to reduced regrowth capacity in mature neurons.** (A–C) Representative microfluidic images (A and B) and quantitative analysis (C) showing reduced capacity of axonal regrowth in mature cortical neurons after axotomy. Neurons were axotomized at DIV4 (A) or DIV12 (B) and imaged by staining of βIII-tubulin 3 (A) or 6 d (B) after injury. Although young neurons at DIV7 maintain some level of regrowth capacity, mature neurons at DIV18 show failed regeneration ($P < 0.001$, Mann–Whitney test). (D and E) Representative immunoblots (D) and quantitative analysis (E) showing progressive increase in SNPH expression with neuron maturation. Cortical neurons isolated from E18 mouse brains were cultured for 3, 7, 9, 12, 15, 18, and 22 d. Equal amounts (20 μg) of cell lysates were loaded and sequentially immunoblotted with various antibodies after stripping between applications of each antibody. Brain lysates from E18 WT, adult WT, and adult *snph* KO mice were used as controls. The intensity of SNPH bands were quantified from three repeats, calibrated with TOM20 levels, and then normalized to SNPH expression at DIV7. (F–H) Kymographs (F) and quantitative analysis (G and H) showing progressive decline of axonal mitochondrial motility with neuron maturation. Cortical neurons were transfected with DsRed-Mito or Rab7-YFP. Time-lapse images, obtained at DIV7, 9, 12, or 18, were recorded for 100 frames with 5-s intervals. In kymographs, vertical lines represent stationary organelles; oblique lines or curves to the right indicate anterograde transport toward distal terminals. Note that axonal mitochondria have progressively reduced motility, whereas late endosomes show no significant change in their motility in the same axons during maturation. Bars, 10 μm. Data were analyzed from the total number of chambers indicated within bars (C) or the total number of neurons indicated within bars (G and H) and expressed as mean ± SE and by one-way ANOVA test.

D). SNPH-mediated suppression of axon regrowth is partially recovered by supplying 200 μM ATP through electroporation (Fig. 3 E). To determine whether mitochondrial ATP production is critical for axon regrowth, we briefly treated the axonal chamber with 2 μM oligomycin, a mitochondrial complex V inhibitor, after axotomy. Such treatment abolishes recovery of the regrowth capacity in *snph* KO neurons (Fig. 3 F). Altogether, these results suggest that supplying ATP to injured axons by enhancing mitochondrial transport contributes to axon regrowth.

To determine whether increased regrowth in *snph* KO neurons is secondary to improved neuronal survival, we examined MAP2-positive survival neurons and TUNEL-positive death cells in the somatic chamber (Fig. S2 A) and characterized the correlation between cell density and axonal regrowth after injury. Our study shows no significant change in the normalized density of MAP2-positive neurons (Fig. S2 B) and percentage of TUNEL-positive death cells (Fig. S2 C) between WT and *snph* KO neurons at 1 h and 3 d after axotomy (P > 0.05). Although WT neuron density correlates with axonal re-

growth after injury ($R^2 = 0.3501$, P < 0.0001), enhanced axonal regrowth in *snph* KO neurons is not correlated with relative cell density in the soma chamber ($R^2 = 0.0556$, P = 0.1187; Fig. S2 D). Our results are consistent with previous studies showing that promoting neuronal survival failed to increase axon regeneration (Park et al., 2008; Hu et al., 2012).

To further test our hypothesis, we examined the regrowth capacity of mature dorsal root ganglion (DRG) neurons isolated from adult WT or *snph* KO mice at postnatal day (P) 60. These adult DRG neurons are well matured and undergo an axotomy-like injury during cell dissociation and culture preparation; axon regrowth occurs from the cell body 1 h after plating on coverslips, thus partially recapitulating an axonal regrowth program in mature neurons after injury. Because almost all processes in DRG neurons are tau-positive axons (Perlson et al., 2009), adult DRG neurons were immunostained with the neuron-specific marker βIII-tubulin. The *snph* KO adult DRG neurons display increased regrowth capacity, as indicated by the total number of axonal intersections when compared with WT
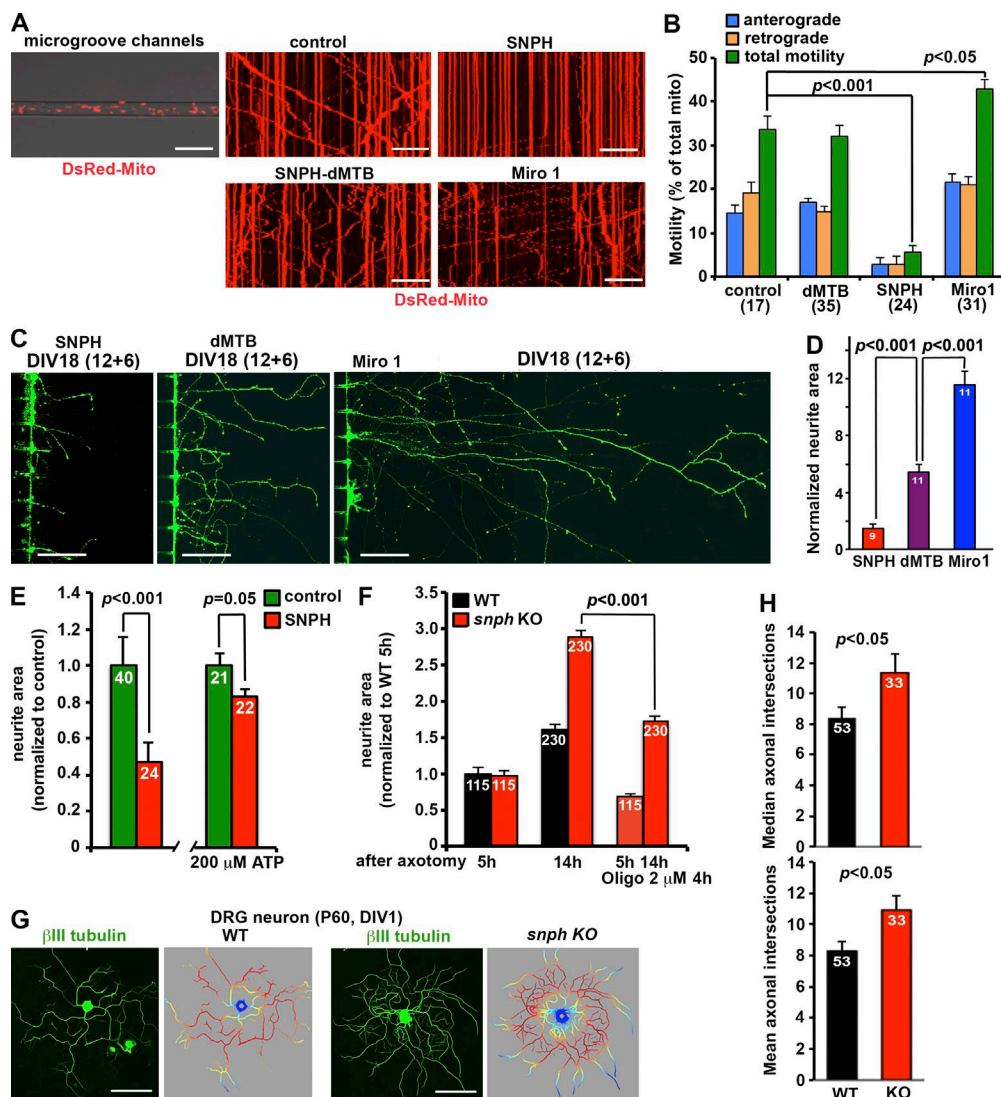
Figure 3. **Mature neurons regain regrowth capacity by enhancing mitochondrial transport.** (A and B) Kymographs (A) and quantitative analysis (B) showing mitochondrial motility along microgrooves in microfluidic chambers. Time-lapse imaging was recorded in cortical neurons at DIV12 for a total of 100 frames with 5-s intervals. In kymographs, vertical lines represent stationary organelles; oblique lines or curves to the right indicate anterograde transport toward distal terminals. Note that the relative motility in control neurons expressing HA is significantly higher than the motility in neurons overexpressing HA-SNPH, but lower than the motility in neurons expressing HA-Miro1. (C and D) Representative microfluidic images (C) and quantitative analysis (D) showing regrowth capacity in mature cortical neurons. Neurons infected with lentivirus encoding SNPH, SNPH-dMTB, or Miro1 were grown on microfluidic chambers for 12 d before axotomy. Axon regeneration was evaluated 6 d after axotomy (DIV18). Note that abolishing mitochondrial transport by expressing SNPH shows failed axon regrowth, whereas enhancing mitochondrial transport by expressing Miro1 robustly increases axon regrowth capacity. (E) Partial recovery of regrowth capacity in the SNPH-expressing neurons by ATP application. The electroporated neurons were immediately plated on a microfluidic chamber with medium containing 200 µM ATP. (F) Recovery of regrowth capacity 14 h after axotomy in *snph* KO neurons is largely abolished by blocking mitochondrial ATP generation with 2 µM oligomycin (Oligo). The axonal chambers were briefly treated with 2 µM oligomycin for 4 h after axotomy. (G and H) Representative images (G) and quantitative analysis (H) showing enhanced axonal regrowth in *snph* KO adult DRG neurons. DRG neurons isolated from adult (P60) WT or *snph* KO mice were immunostained with βIII-tubulin at DIV1. Axon regrowth was quantified by Sholl analysis. The *snph*-deficient adult DRG neurons display increased axon branching as indicated by the total number of axonal intersections. Mitochondrial motility data were analyzed from the total number of microgrooves (B); axonal regrowth data were analyzed in terminal chambers where new axons grow from a total number of microgrooves (E and F), total number of terminal chambers (D), or total number of DRG neurons (H) indicated within bars or in parentheses and expressed as mean ± SE and by one-way ANOVA test (B and D), Student's *t* test (F and H), or Mann–Whitney *U* test (E). Bars: (A) 20 µm; (C and G) 100 µm.

DRG neurons (P < 0.05; Fig. 3, G and H), thereby confirming that axonal regrowth in matured neurons is facilitated by enhancing mitochondrial transport.

Expressing SNPH alters mitochondrial distribution and ATP/ADP ratio in distal axons

A critical step for inducing axon regrowth is the transformation of the injured axonal end into a growth cone–like structure that can integrate extracellular and intracellular signals for regrowth (see reviews by Tessier-Lavigne and Goodman [1996], Yu and Bargmann [2001], and Liu et al. [2011]). We next addressed whether altered mitochondrial motility regulates their distribution in distal axons, thus controlling the size of growth cones in both the peripheral nervous system (PNS) and CNS. We first used adult DRG sensory neurons isolated from adult P60 mice. Neurons were cotransfected with DsRed-Mito with GFP and SNPH, SNPH-dMTB, or Miro1, followed by immunostaining
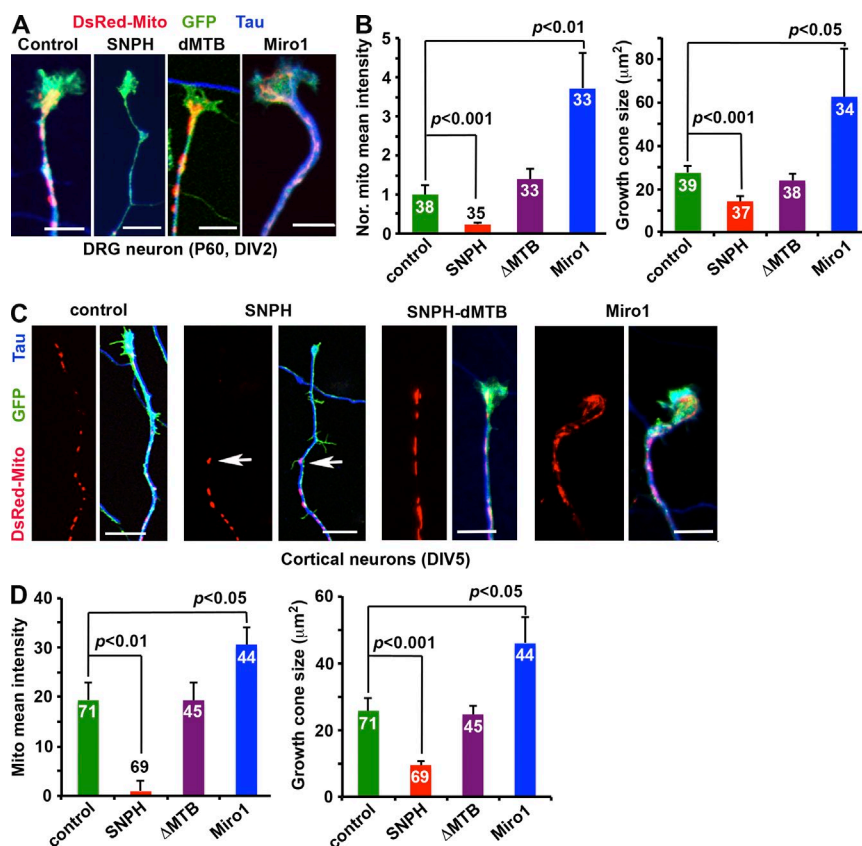
Figure 4. **Mitochondrial transport impacts terminal mitochondrial recruitment and growth cone size.** (A and B) Representative images (A) and quantitative analysis (B) showing correlation of mitochondrial density in the axonal terminals and growth cone size of adult DRG neurons after dissociation axotomy. Adult DRG neurons isolated from P60 mice were cotransfected with DsRed-Mito, GFP, and control vector, SNPH, SNPH-dMTB, or Mrio1, followed by immunostaining with Tau at DIV2. Note that expressing SNPH, but not its loss-of-function mutant SNPH-dMTB, blocks the delivery of mitochondria into growth tips and reduces average size of growth cones, whereas expressing Miro1 robustly increases terminal mitochondrial density and size of growth cones. (C and D) Images (C) and quantitative analysis (D) of distal mitochondrial distribution and growth cone size in cortical neurons coexpressing DsRed-Mito with GFP or together with SNPH, SNPH-dMTB, or Miro1. Neurons at DIV5 were immunostained with Tau. Note that both mitochondrial density in terminals and the average size of growth cones are decreased in neurons expressing SNPH ($P < 0.01$ and $P < 0.001$, respectively), but increased in neurons expressing Miro1 ($P < 0.05$) relative to control neurons. Arrows indicate the most distal mitochondrion in the SNPH-expressing axons (C). Data were analyzed from the total number of axons indicated within bars from more than three experiments and expressed as mean ± SE and by one-way ANOVA test. Bars, 10 μm.

with the axonal marker Tau. Expressing SNPH, but not its loss-of-function mutant dMTB, blocks delivery of mitochondria into axonal terminals (Fig. 4, A and B). Conversely, expressing Miro1 increases mitochondrial density in growth cones. Interestingly, these mitochondrial distribution patterns correlate with the mean size of reformed growth cones in adult DRG neurons after dissociation axotomy.

We further confirmed this correlation in cortical neurons by coexpressing DsRed-Mito with GFP or together with SNPH, SNPH-dMTB, or Miro1, followed by immunostaining with Tau. Both mitochondrial density in axonal terminals and the mean size of growth cones were decreased in neurons overexpressing SNPH ($P < 0.01$ and $P < 0.001$, respectively), but increased in neurons overexpressing Miro1 ($P < 0.05$) relative to control neurons (Fig. 4, C and D). Because SNPH is hardly detectable before DIV7, it is predictable that expressing loss-of-function mutant SNPH-dMTB in young cortical neurons (DIV5) displays no dominant-negative effect on mitochondrial density nor the mean size of growth cones when compared with control neurons (Fig. 4 D). Thus, our results provide a clue as to why an injured axonal tip in mature neurons often fails to transform into an active growth cone (Li and Raisman, 1995; Hill et al., 2001), as mitochondrial recruitment is suppressed by elevated SNPH expression.

Reduced mitochondrial density within axonal terminals in the SNPH-expressing neurons prompted us to examine how mitochondrial motility impacts ATP homeostasis throughout an axon. The cellular ATP/ADP ratio in live axons was measured by applying an engineered fluorescent ATP sensor, PercevalHR, in live neurons (Sun et al., 2013; Tantama et al., 2013). The fluorescence intensity ratio (F_{488nm}/F_{405nm}) reflects the relative ATP/ADP ratio, thus allowing spatial detection of intracellular

ATP homeostasis in various axonal segments. Relative mitochondrial density and ATP/ADP ratios along an axon were analyzed based on five equally divided segments of each individual axon from the most proximal to the most distal region (Fig. S3, A and B). Overexpressing SNPH in cortical neurons redistributes axonal mitochondria to the proximal region ($P < 0.001$) and also reduces mitochondrial density and the ATP/ADP ratio in the most distal axon segment ($P < 0.001$ and $P < 0.05$, respectively). Because intracellular pH values impact the Perceval fluorescent intensity (Berg et al., 2009), we monitored pH in axons using the pH dye SNARF-5F (Fig. S3, C and D). SNARF-5F signal was calibrated using various buffered solutions containing high K$^+$/nigericin with varying pH values (Fig. S3, E and F). The pH values in an entire axon of both WT and SNPH overexpression neurons undergo very minor changes (7.10–7.15). Thus, reduction in the ATP/ADP ratios in distal axons is physiologically relevant to the reduced axonal mitochondrial density. These results suggest that proper mitochondrial positioning in distal axons is required to maintain local ATP homeostasis. Therefore, in mature neurons, where SNPH expression is elevated and axonal mitochondrial motility is suppressed (Fig. 2), local ATP deficits occur if injury stress triggers mitochondria dysfunction. This notion is supported by previous in vivo studies showing that axonal injury induces mitochondrial depolarization and oxidative stress (O'Donnell et al., 2013; Cavallucci et al., 2014).

Axotomy triggers an acute stress signal that depolarizes local mitochondria

We assessed the impact of axotomy on mitochondrial integrity by performing the following four experiments. First, we chose adult DRG neurons for laser-based axotomy using a multitimer programed two-photon laser microsurgery as previously

described (Cho et al., 2013) with some modifications. A train of near-infrared femtosecond laser pulses lead to nearly 100% physical separation of axonal processes. Time-lapse images demonstrate that although mitochondria at the axotomized site were ablated during axotomy, mitochondria in the vicinity suddenly shrank and lost their staining by tetramethylrhodamine ethylester (TMRE), a fluorescent dye that stains mitochondria depending on membrane potential ($\Delta\psi_m$; Fig. 5, A–C).

Second, we confirmed the axotomy-induced depolarization of local mitochondria in mature cortical neurons on microfluidic chambers. Neurons were infected with lentiviruses expressing pLenti-GFP or pLenti-GFP-Mito. Axon bundles in the terminal chambers were loaded with 25 nM TMRE dye at DIV12, followed by laser-based axotomy and time-lapse imaging. The axons were quickly broken up during axotomy, and mitochondria in the vicinity suddenly lost their TMRE staining (Fig. 5 D and Video 6). Similarly, in the axons expressing GFP-Mito, axotomy triggered a loss of TMRE staining near the axotomy site, while those depolarized mitochondria still maintained GFP-Mito signals (Fig. 5 E and Video 7). Alternatively, we applied a physical axotomy in the axonal chamber by using pulled glass capillaries with a tip diameter of ∼1 µm. Neurons were loaded with both TMRE ($\Delta\psi_m$-dependent dye) and MitoTracker Green FM ($\Delta\psi_m$-independent dye) before axotomy. After physical axotomy, TMRE staining was lost near the axotomized ends, whereas MitoTracker Green FM staining remained (Fig. S4 A). In addition, we costained mitochondria in the axonal chambers with MitoTracker Green FM and MitoTracker Red FM ($\Delta\psi_m$-insensitive dye with similar wavelength as TMRE). Laser-induced axotomy does not reduce the signal intensity of MitoTracker Red FM (Fig. S4 B), thus excluding an artificial laser effect on TMRE signals.

Third, we examined somatic mitochondrial integrity by staining with MitoTracker Orange CMTMRos, a fixable $\Delta\psi_m$-dependent dye. Axotomy in the axonal terminal chamber does not induce any observable reduction in the mean intensity of Orange CMTMRos in the soma chamber at 1 and 5 h after injury (Fig. S4 C). In addition, we asked whether the observed local mitochondrial damage is accompanied by ATP depletion in the injured axons. To monitor intracellular ATP levels, we applied the red-shifted genetically encoded ATP probe GO-ATeam2, in which GFP and OFP were used as a FRET (Förster resonance energy transfer) pair (Nakano et al., 2011). This ATP probe is relatively stable against acidification and less phototoxic to cells and thus is suitable for long-time live imaging. Laser-based axotomy triggers a quick ATP depletion at millimolar levels in the vicinity of the injured site of adult DRG neurons (Fig. 5, F and G), indicating axotomy-induced energy deficits. These studies consistently support the notion that axotomy is an acute stress signal that depolarizes local mitochondria, thus triggering energy deficits in the vicinity of injury sites.

Enhanced transport recovers mitochondrial integrity and rescues energy deficits

Depolarized mitochondria not only supply less ATP, but also release toxic reactive oxygen species that trigger axon degeneration (Sheng and Cai, 2012). Therefore, quickly replacing those damaged mitochondria not only protects axons from degeneration, but also supports high-energy demanded regeneration. We hypothesize that the intrinsic reduction of mitochondrial transport in mature neurons impairs efficient delivery of healthy mitochondria to and removal of damaged mitochondria from in-

jured axons. Mature cortical neurons can regain axon regrowth capacity by enhancing mitochondrial transport (Fig. 1, C–E; and Fig. 3 C), supporting that proper axonal transport is essential to maintain mitochondrial integrity and energy supply in response to injury-induced mitochondrial damage.

To test our hypothesis, we performed the following three types of experiments. First, we characterized axonal mitochondrial flux along the microgrooves before and after axotomy in WT and *snph* KO mature cortical neurons infected with pLenti-GFP-Mito. Mitochondrial flux was measured by the total number of bidirectional transport events through the microgrooves. Deleting *snph* significantly increases axonal mitochondrial flux before (P < 0.001) and 10 min (P < 0.05) and 1 h after axotomy (P < 0.001) when compared with WT neurons (Fig. 6, A and B; and Videos 8 and 9). Our findings also suggest that the immediate pause of axonal mitochondria upon axotomy (Videos 6 and 7) is likely a temporary response to high calcium influx into injured axons; paused mitochondria are then recruited to motile pools 10 min after axotomy, and their total flux rate is affected by the relative SNPH expression in mature neurons.

Next, we investigated the impact of enhanced transport on the recovery of mitochondrial integrity by examining mitochondrial $\Delta\psi_m$ after injury. Cortical neurons were infected with pLenti-GFP-Mito and axons were loaded with 25 nM TMRE dye before or 1 or 5 h after axotomy. Axotomy impairs mitochondrial integrity by depolarizing $\Delta\psi_m$ in the proximal ends of the injured axons in WT neurons (Fig. 6 C). However, there was a significant increase (P < 0.001) in TMRE recovery in *snph* KO neurons (Fig. 6 D), suggesting that the mitochondrial stress phenotype can be reversed in *snph* KO axons by enhanced mitochondrial transport. These results support our hypothesis that enhancing mitochondrial transport helps remove damaged mitochondria and/or replenish healthy ones to the proximal ends of injured axons.

We next asked whether local ATP deficits occur after axotomy-induced mitochondrial dysfunction in mature neurons, where SNPH expression is elevated and axonal mitochondrial motility is suppressed (Fig. 2). We measured ATP maintenance in the distal growing tips 6 h after axotomy in WT and *snph* KO neurons infected with pLenti-PercevalHR. Enhanced mitochondrial transport in *snph* KO axons significantly increases the ATP/ADP ratio in the growing tips relative to that in WT neurons (Fig. 6, E and F). We detected no change in pH values at growing tips 6 h after axotomy between WT and *snph* KO neurons (Fig. S5 A). To further confirm these observations, we alternatively applied the ATP probe GO-ATeam2 to monitor intracellular ATP levels by measuring the F_{560nm}/F_{510nm} ratiometric integrated intensity before or 1, 3, or 5 h after axotomy. ATP-insensitive GO-ATeam3 mutant (R122K/R126K; Nakano et al., 2011) was also applied as a control of imaging and axotomy procedures. WT neurons expressing the ATP probe GO-ATeam2 display reduced F_{560nm}/F_{510nm} integrated intensity in the distal microgrooves after axotomy, suggesting an axotomy-induced ATP depletion. Enhancing axonal mitochondrial transport in *snph* KO neurons recovers energy deficits at 3 and 5 h after axotomy (Fig. 6, G and H; and Fig. S5 B). As a control, WT neurons expressing ATP-insensitive GO-ATeam3 mutant do not show any significant change after axotomy (Figs. S5, C and D). Thus, both ATP sensors Perceval and GO-ATeam2 consistently reveal a higher ATP/ADP ratio in the regrowing axon of *snph* KO neurons than in those of WT neurons after axotomy. We further confirmed that enhancing mitochondrial transport
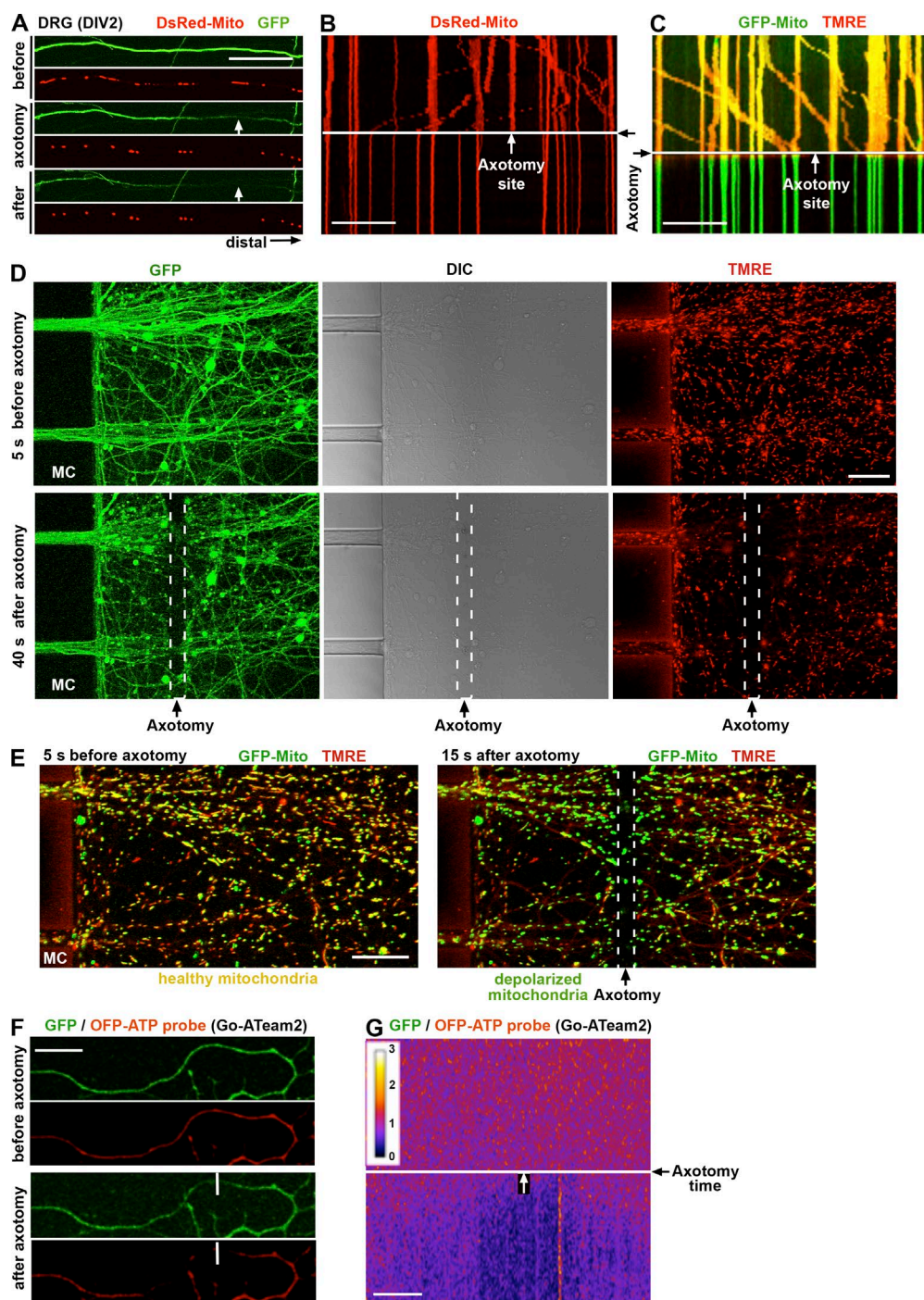
Figure 5.   **Axotomy depolarizes mitochondria in the vicinity of injured sites.** (A) Representative images showing axonal mitochondria in adult DRG neurons before and after laser-based axotomy. Adult DRG neurons isolated from P60 mice were cotransfected with DsRed-Mito and GFP. Note that mitochondria at the axotomized site were immediately lost during axotomy (white arrows). (B and C) Kymographs showing axonal mitochondria labeled by DsRed-Mito (B) or cola-beled by GFP-Mito and TMRE (C) before and after axotomy. The white arrows indicate laser-scanning sites (injured site), and the black arrows in the y axis show the laser execution time. Time-lapse images were captured to show that mitochondria in the vicinity suddenly shrunk (B) and lost the $\Delta\psi_m$ (TMRE staining; C). The images were first recorded at 5-s intervals for a total of 50 frames; the consecutive post-axotomy recording was collected at 5-s intervals for a total of 50 frames. (D and E) Representative images showing axotomy-induced depolarization of axonal mitochondria. Neurons were infected with pLenti-GFP (D) or GFP-Mito (E), and axons in the terminal chambers were loaded with 25 nM TMRE dye at DIV12, followed by laser-based axotomy and time-lapse imaging. Note that in neurons expressing GFP (D), axons were quickly broken up upon axotomy (white dashed lines), and a majority of mitochondria in the vicinity suddenly lost their TMRE staining (bottom right). In neurons expressing GFP-Mito (E), axotomy triggered a sudden loss of mitochondria staining by TMRE near the axotomy site (white dashed lines), whereas those depolarized mitochondria maintained GFP-Mito signals. MC, microgroove channels. (F and G) Representative images (F) and ratiometric kymograph (G) showing axotomy-induced ATP depletion. Cultured adult DRG neurons from 2-mo-old mice were transfected with red-shifted ATP probe GO-ATeam2, in which GFP and OFP were used as a FRET pair to monitor intracellular ATP levels with an affinity K_d of 2.3 mM at 37°C. Laser-based axotomy was applied (white bars in F, white arrow in G) along a distal axon. The green color is the cp173-mEGFP channel, and the red color is the OFP channel (mKOk). The ratiometric kymograph was generated by time-lapse imaging of a total of 100 frames with 5-s intervals. Axotomy was applied at the 51th frame (G). Note that axotomy triggers acute ATP depletion at millimolar levels in the vicinity of the injured site. Bars: (A–C) 10 µm; (D–G) 20 µm.
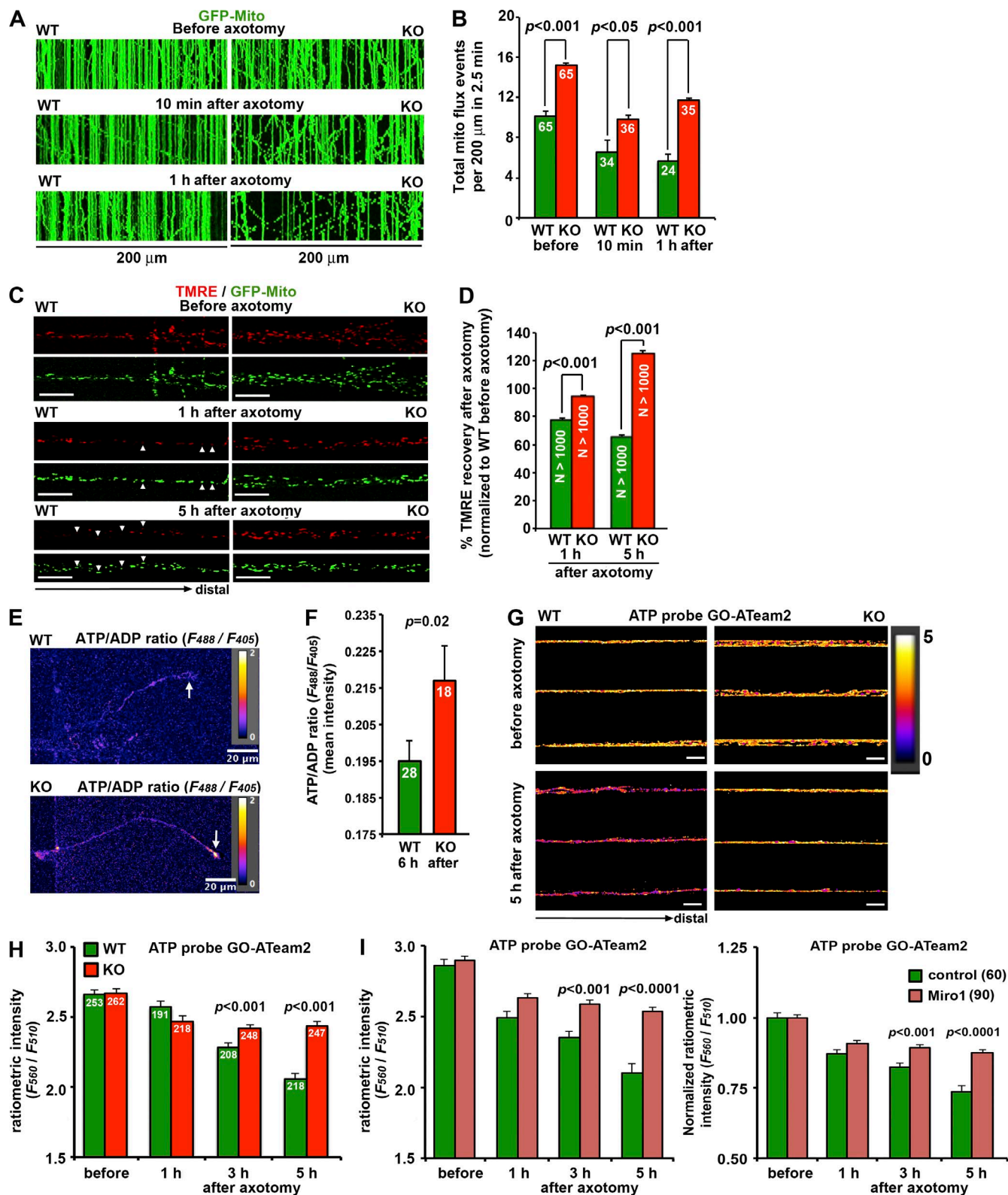
Figure 6. **Enhanced mitochondrial transport recovers mitochondrial integrity and rescues energy deficits in injured axons.** (A and B) Kymographs (A) and quantitative analysis (B) showing axonal mitochondrial flux of WT and *snph* KO cortical neurons along microgrooves. Neurons were infected with pLenti-GFP-Mito. Time-lapse imaging was recorded for 30 frames with a 5-s interval for a total of 2.5 min. In kymographs, vertical lines represent stationary organelles; oblique lines or curves to the right indicate anterograde transport toward terminals. The mitochondrial flux in axonal bundles was measured by the total events of bidirectional transport through microgrooves. The images were acquired by 40× lens. Note that deleting *snph* significantly increases axonal mitochondrial flux before and after axotomy when compared with WT neurons. Data were analyzed from the total number of microgrooves indicated within bars from more than three independent experiments and expressed as mean ± SE and by Student's *t* test. (C and D) Images (C) and quantitative analysis (D) showing the recovery of TMRE staining on axonal mitochondria in the microgrooves adjacent to the axotomized site. Cortical neurons were infected

in WT neurons by overexpressing Miro1 also recovers axotomy-induced energy deficits (Fig. 6 I). Our study thus highlights the crucial role of mitochondrial transport in maintaining ATP supply in response to axotomy-induced mitochondrial damage.

To examine whether adult *snph* KO neurons display any altered capacity of calcium buffering, we applied the green fluorescent Ca²⁺ sensor G-GECO1.2 with a $K_d = 1.15$ μM (Zhao et al., 2011), a Ca²⁺ sensor well characterized in our previous study (Di Giovanni and Sheng, 2015). The sensor G-GECO1.2 was electroporated into neurons and imaged 2 d later. The multi-timer macro was applied for consecutive laser axotomy and image acquiring of calcium buffering capacity (Fig. S5 E). The maximal length of Ca²⁺ sensor response was unchanged after deleting *snph* (P = 0.423; Fig. S5 F). The mean decay time constant within 40 μm of the proximal end of injured axons, calculated based on the florescence intensity (F/F_0) curve with a nonlinear fit, showed no significant change (WT: 15.28 ± 0.08; KO: 15.57 ± 0.08, P = 0.827; Fig. S5 G). Thus, Ca²⁺ sensing is unlikely the key pathway in *snph* KO neurons to facilitate axonal regrowth after injury.

snph KO sciatic nerves display enhanced regenerative capacity in vivo after injury

Our ex vivo imaging in adult *snph* KO mice (2 mo old) displays enhanced mitochondrial motility along axonal bundles of sciatic nerve (71.58 ± 2.72%, P < 0.0001) relative to those from control littermates (30.948 ± 2.17%; Videos 1 and 2). To test whether enhanced mitochondrial transport facilitates axonal regeneration in vivo, we crushed sciatic nerve in adult *snph* KO mice and control littermates (2 mo old) and assessed the level of regeneration past the crush site 3 d after injury. We first verified SNPH depletion in *snph* KO sciatic nerve by co-immunostaining SNPH and βIII-tubulin. Although SNPH-targeted mitochondria are abundant along the axons of sciatic nerves of WT mice, SNPH staining was absent in the same region of *snph* KO mice (Fig. 7 A).

To visualize regrowth of damaged axons in vivo, longitudinal sciatic nerve sections were stained for the growth-associated protein, GAP-43. The reported concentrations of GAP-43 in growth cones (Goslin et al., 1988) and regenerating axons (Fu and Gordon, 1997) make it an ideal marker to track axon regeneration in vivo (Ackermann et al., 2002; Abe et al., 2010). GAP-43 expression was undetectable or at a very low level in the axons of uninjured WT and *snph* KO sciatic nerve (Fig. 7 B). Adult WT and *snph* KO mice were subjected to a sciatic nerve crush injury and axonal regenerative capacity 3 d after the crush injury was assessed in sciatic nerve longitudinal

sections by examining GAP-43–positive axonal processes. The length of GAP-43–expressing axons past the crush site was significantly increased in *snph* KO sciatic nerves compared with that of control littermates (Fig. 7 C). We quantified this increase by normalizing the number of GAP-43–expressing axons at various distances from the crush site. *snph* KO sciatic nerves display significantly more regenerating axons at 1.5 (P < 0.001), 2.0 (P < 0.01), 2.5 (P < 0.01), and 3.0 mm (P < 0.001) distal from the crush site than WT controls (Fig. 7 D). In addition, we calculated a regeneration index by measuring the distance away from the crush site in which the average number of GAP-43–positive axons is half of that observed at the crush site. The regeneration index is significantly higher in *snph* KO sciatic nerve compared with that of WT (P = 0.01, Student's *t* test; Fig. 7 E). Thus, our in vivo crush study suggests that enhanced axonal mitochondrial transport in *snph* KO sciatic nerves accelerates axon regeneration.

Next, we examined whether rescued energy deficits in mature *snph* KO neurons impact GAP-43 expression in both injured ipsilateral and uninjured contralateral DRG neurons 3 d after injury. Although WT contralateral DRG neurons display undetectable or low levels of GAP-43, sciatic nerve injury induces its expression in ipsilateral DRG neurons (Fig. 8, A and B), consistent with injury-induced GAP-43 expression. To our surprise, GAP-43 expression in *snph* KO DRGs is increased to a larger extent after injury. Although a significant number of uninjured contralateral DRG neurons express GAP-43, which mimics the peripheral conditioning lesion effect, sciatic nerve injury further enhances its expression. Elevated GAP-43 expression is induced in association with nerve regeneration, potentially recapitulating an early developmental program. Enhanced axonal mitochondrial transport and rescued energy deficits in mature *snph* KO neurons likely activate the early intrinsic program to support neuron regrowth.

Discussion

In the current study, we reveal a previously unknown cellular pathway that controls axonal regenerative capacity in mature neurons. Although mitochondrial transport in axons progressively declines with neuron maturation, axonal injury triggers an acute stress signal that depolarizes local mitochondria, leading to energy deficits near the injured site. Thus, maintaining a local ATP supply via recruiting healthy mitochondria into injured axons is critical to meet the enhanced metabolic requirements during axonal regeneration. Enhancing mitochondrial transport

with pLenti-GFP-Mito, and axon bundles were loaded with 20 nM TMRE dye before or 1 or 5 h after axotomy. Live images were acquired at 12 bit below the saturate setting for quantitative analysis of $\Delta\psi_m$ of individual GFP-Mito–labeled mitochondria in axon bundles. Note that axotomy impairs mitochondrial integrity by depolarizing $\Delta\psi_m$ (reduced TMRE staining, arrowheads) in the distal axons of WT neurons; the phenotype can be effectively reversed by enhanced mitochondrial transport in *snph* KO axons. Data were analyzed from the total number of mitochondria (n > 1,000) for each condition indicated within bars. (E and F) Pseudo-color images (E) and quantitative analysis (F) showing ATP maintenance in the growing tips 6 h after axotomy in WT and *snph* KO neurons infected with pLenti-PercevalHR. The F_{488nm}/F_{405nm} ratiometric mean intensity of PercevalHR reflects the relative ATP/ADP ratio. Note that enhanced mitochondrial transport in *snph* KO axons increases the ATP/ADP ratio in the growing tips (white arrows). (G and H) Pseudo-color ratiometric images (G) and the F_{560nm}/F_{510nm} ratiometric integrated intensity (H) of ATP probe GO-ATeam2. Both WT and *snph* KO cortical neurons were transfected with ATP-sensitive GO-ATeam2 probe, followed by imaging distal 150-μm microgrooves before or 1, 3, or 5 h after axotomy. Note that WT neurons display reduced F_{560nm}/F_{510nm} integrated intensity after axotomy, suggesting ATP depletion. Enhancing mitochondrial transport in *snph* KO neurons reverses energy deficits. (I) Overexpressing Miro1 rescues axotomy-induced energy deficits. Quantitative analysis shows the F_{560nm}/F_{510nm} ratiometric integrated intensity (left) and normalized F_{560nm}/F_{510nm} integrated intensity (right) of ATP probe GO-ATeam2. WT neurons were coinfected with lenti–GO-ATeam2 and lenti-control vector or lenti-Miro1 at DIV0, followed by axotomy at DIV8 and imaging of distal 150-μm microgrooves before or 1, 3, or 5 h after axotomy. Note that enhancing mitochondrial transport in WT neurons expressing Miro1 recovers energy deficits. Data were analyzed from the total number of microgrooves indicated within bars or in parentheses and expressed as mean ± SE and Mann–Whitney *U* test (F) or Student's *t* test (D, H, and I). Bars, 20 μm.
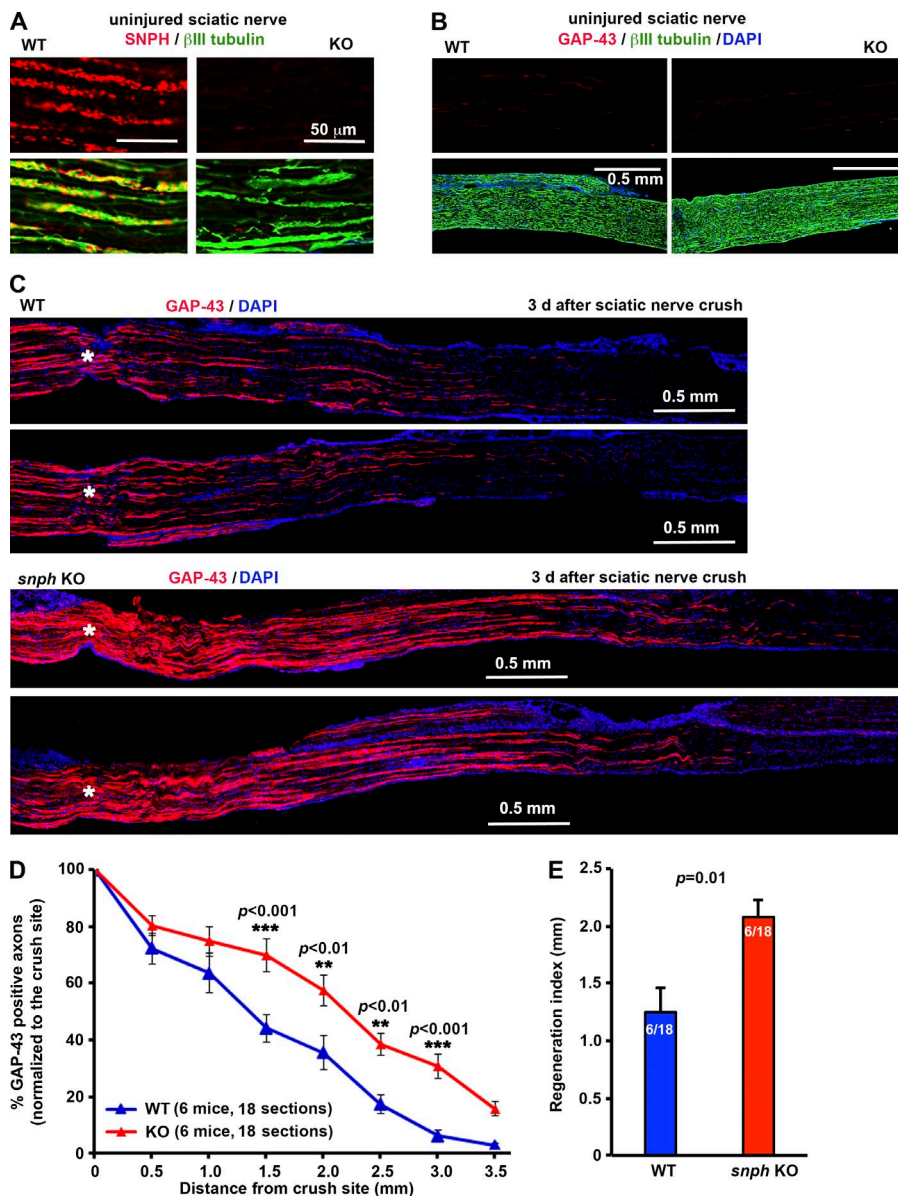
Figure 7. SNPH KO sciatic nerves display enhanced regenerative capacity after crush injury. Adult WT and *snph* KO mice (2 mo old) were subjected to a sciatic nerve crush injury and sacrificed at 3 d after injury. Regenerating axons through and beyond the lesion site were visualized by their expression of GAP-43 on sciatic nerve longitudinal sections. DAPI was used to label the cell nuclei. Sciatic nerves from the contralateral side were used as uninjured controls. (A) Although SNPH-labeled mitochondria are abundant along the axons (labeled by βIII-tubulin) of the uninjured WT sciatic nerve, SNPH staining was absent in the same region of *snph* KO mice. (B) Expression of GAP-43 was undetectable in the uninjured sciatic nerve axons of WT and *snph* KO mice. (C) Representative images of sciatic nerve longitudinal sections show GAP-43–positive regenerating axons. Note that at 3 d after the crush injury, *snph* KO mice display a marked increase in the number and growth distance of GAP-43–positive axons past the injury site as compared with the WT littermates. The crush site is indicated by asterisks. (D) Quantification of GAP-43–positive axons in the distal sciatic nerves reveals that regenerating axons grew significantly longer distances at 3 d after injury in *snph* KO mice than WT controls. The number of GAP-43–positive axons at various distances from the crush site was counted and normalized to the crush site. Note that *snph* KO mice display significantly more regenerating axons at 1.5 (***, $P < 0.001$), 2.0 (**, $P < 0.01$), 2.5 (**, $P < 0.01$), and 3.0 mm (***, $P < 0.001$) distal to the crush site (two-way ANOVA, followed by Bonferroni's post-hoc test). (E) The regeneration index was measured as the distance away from the crush site in which the mean number of regenerating axons is half of that observed at the crush site. *snph* KO sciatic nerves show a higher regeneration index compared with WT ($P = 0.01$, Student's *t* test). Data are mean ± SE ($n = 6$ mice per genotype and 3 longitudinal sections per animal).

not only helps remove those injury-damaged mitochondria, but also replenishes healthy ones in the injured axons, thus recovering mitochondrial integrity and reversing energy deficits. This cellular process is critical for mature neurons to facilitate their regeneration after injury (Fig. 9). Therefore, our study provides new mechanistic insights as to how mature neuron-associated elevation of SNPH expression contributes to regeneration failure. Thus, rescuing local energy deficits by enhancing mitochondrial transport is one of the potential cellular targets for new therapeutic strategies to stimulate axon regeneration.

Energy deficits in injured axons contribute to regeneration failures

CNS injury in adult mammals usually leads to a failure to initiate regeneration because of an inability to assemble a new active growth cone, a cellular process that includes sealing ruptured membranes, retrograde growth signaling, cytoskeleton restructuring, local translation, transport of building materials, and insertion of new membrane and cell surface molecules (Bradke et al., 2012). All of these steps demand high energy consumption. ATP consumption is central to axon growth and regeneration. Mitochondrial ATP production provides most of the axonal energy. Because the diffusion capacity of intracellular ATP through long axons is rather limited (Sun et al., 2013), local mitochondria provide the ATP necessary to support axonal regeneration. Axonal injury induces mitochondrial depolarization and oxidative stress associated with axonal degeneration (O'Donnell et al., 2013; Cavallucci et al., 2014). Therefore, proper mitochondrial transport into regenerating axons ensures that metabolically active areas are adequately supplied with ATP. Thus, ATP consumption and supply are central to axon regeneration.

Our study demonstrates that both physical and laser-based axotomy triggers an acute stress signal that efficiently depolarizes local mitochondria (Fig. 5 and Fig. S4), thus reducing ATP supply to the growing tips after injury (Fig. 6 and Fig. S5). Mitochondrial dysfunction and impaired transport are associated with the pathology of neurodegenerative disorders (see reviews by Chen and Chan [2009], Court and Coleman [2012], and Sheng and Cai [2012]). Dysfunc-
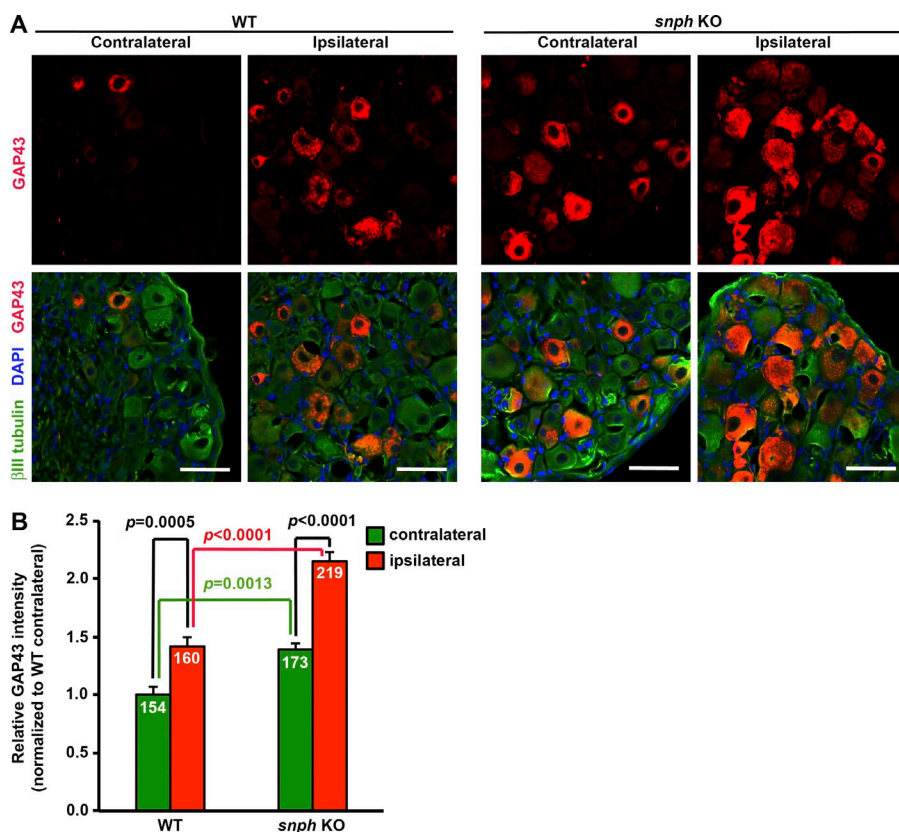
A

	WT		snph KO	
	Contralateral	Ipsilateral	Contralateral	Ipsilateral

GAP43

βIII tubulin DAPI GAP43

B

Relative GAP43 intensity (normalized to WT contralateral)

p=0.0005, p<0.0001, p<0.0001, p=0.0013

- contralateral
- ipsilateral

WT: 154, 160
snph KO: 173, 219

Figure 8. **Relative expression of GAP-43 after sciatic nerve injury.** (A and B) Representative images (A) and quantitative analysis (B) show increased GAP-43 expression in *snph* KO DRG neurons. *snph* KO and WT littermates (9 wk old) were subjected to a left-sided sciatic nerve injury. Both injured ipsilateral and uninjured contralateral L5 DRGs of WT and *snph* KO mice were co-immunostained with antibodies against GAP-43, βIII-tubulin, and DAPI 3 d after crush injury. Note that in *snph* KO mice, a higher GAP-43 expression is detected in uninjured DRGs (contralateral) as compared with the WT mice (P = 0.0013). GAP-43 expression is further increased in response to the sciatic nerve injury in *snph* KO mice (P < 0.0001). Data were analyzed from the total number of neurons indicated within bars from four mice for each genotype and expressed as mean ± SE and by two-way ANOVA followed by Tukey's post-hoc test. Bars, 50 μm.

tional mitochondria not only supply less ATP, but also release toxic reactive oxygen species and apoptotic factors, which further trigger axonal pathology and degeneration (Lucius and Sievers, 1996; Koeberle and Ball, 1999; Alvarez et al., 2008). We show that SNPH-mediated mitochondrial anchoring in mature axons impairs delivery of healthy mitochondria to and removal of those damaged mitochondria from injured axons, thus leading to energy deficits and loss of regrowth capacity. However, the mitochondrial stress and energy deficits at the injured axons can be effectively rescued by enhanced mitochondrial transport in axons (Fig. 6). Efficiently replacing those damaged mitochondria serves as a neuroprotective mechanism essential for regeneration.

Mature neuron-associated elevation of SNPH expression inhibits regenerative capacity

The majority of axonal mitochondria are stationary in mature neurons, which is achieved through an SNPH-mediated anchoring mechanism. SNPH targets axonal mitochondria through its carboxyl-terminal mitochondria-targeting domain and immobilizes mitochondria by anchoring to MTs (Kang et al., 2008; Chen and Sheng, 2013). Deleting *snph* results in a robust increase of axonal mitochondrial transport. Conversely, overexpressing SNPH abolishes mitochondrial transport in axons. Strikingly, SNPH is strictly developmentally regulated in brains: its expression is hardly detectable in embryonic stages and before P7 and peaks 2 wk after birth (Das et al., 2003). Here, we further reveal mature neuron-associated SNPH expression (Fig. 2, D and E). As a result, axonal mitochondria display progressively reduced motility during maturation from DIV7 to DIV18 (Fig. 2, F and G). This unique SNPH expression highlights a new intrinsic pathway controlling axonal regrowth capacity: increased

SNPH expression in mature neurons and reduced mitochondrial transport account for the mature neuron-associated decline of regenerative capacity. Therefore, the *snph* KO mouse is an ideal genetic model to examine the impact of enhanced mitochondrial transport on in vitro regrowth of mature neurons and in vivo regeneration in adult mice.

We found that when mitochondrial transport is abolished by genetic manipulation, axon regrowth fails after axotomy. Conversely, enhancing mitochondrial transport in mature neurons significantly increases axon regrowth in vitro and regeneration in vivo after injury (Figs. 3 and 7). Such regrowth recovery depends on mitochondrial ATP production: (a) blocking mitochondrial ATP generation abolishes the regrowth recovery in *snph* KO neurons, and (b) applying ATP to neurons overexpressing SNPH partially recovers regrowth capacity. Altogether, these in vitro and in vivo studies suggest that maintaining the ATP supply to injured axons by enhancing mitochondrial transport facilitates axonal regeneration.

Mitochondrial flux into distal axons supports axonal growth and branching during early brain development (Morris and Hollenbeck, 1993; Spillane et al., 2013; Tao et al., 2014). A recent study highlights a critical role for SNPH-mediated mitochondrial anchoring in the maintenance of axonal branching through the AMPK signaling pathway (Courchet et al., 2013). Activation of AMPK increases anterograde flux of mitochondria into axons and induces axonal branching in an ATP-dependent manner. As a cellular energy sensor, AMPK activation may regulate signaling pathways that replenish ATP supplies. Although these studies focused on axonal growth in developing neurons, a fundamental question remains unaddressed: does mitochondrial transport play a critical role in the facilitation of axonal regeneration in mature neurons? The *snph* KO neurons show no detectable changes in initial axon growth during early de-
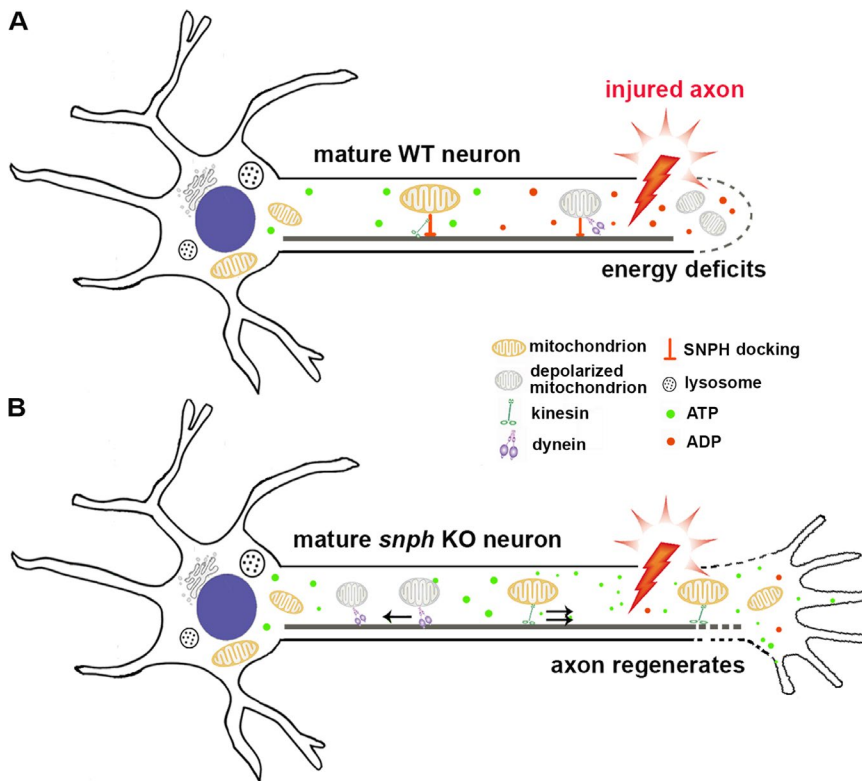
Figure 9. **Model illustration of enhanced mitochondrial transport critical for mature neurons to regain axonal regenerative capacity.** (A) Although mitochondrial transport in WT axons progressively declines with maturation, axonal injury depolarizes local mitochondria, thus leading to energy deficits. Energy deficits may reflect the intrinsic restriction of mature axons to regenerate after injury. (B) Enhanced local ATP supply via healthy mitochondrial flux into injured axons is critical to meet metabolic requirements for axonal regeneration. Enhancing mitochondrial transport in *snph* KO axons not only helps remove those dysfunctional mitochondria, but also replenishes healthy ones to the injured axons, thus recovering mitochondrial integrity and rescuing energy deficits.

velopmental stages when compared with WT neurons (Fig. S1, A and B; Kang et al., 2008); this is attributed to the fact that SNPH is hardly detectable during early development (Fig. 2, D and E). Thus, the SNPH-mediated mechanism controls axonal regrowth/regeneration in mature neurons, rather than initial growth in developing neurons.

Selection of in vivo system for injury-induced regeneration

The failure of CNS regeneration is caused by a lack of induction of a cell-intrinsic growth capacity after injury (Afshari et al., 2009; Giger et al., 2010) and the presence of extrinsic inhibitory effects (Filbin, 2006; Yiu and He, 2006; Hoffman, 2010; Sun et al., 2011). In view of these, we considered that enhancing mitochondrial transport and rescuing energy deficits may not be sufficient to activate intrinsic signaling pathways and overcome extrinsic inhibitory effects in the CNS. In contrast, injured axons in the adult PNS maintain some capacity to regenerate (Abe and Cavalli, 2008; Chandran et al., 2016). We reasoned that regenerative capacity in PNS could be further facilitated in *snph* KO mice if enhanced mitochondrial transport rescues local energy deficits after injury. Thus, by focusing on the sciatic nerve crush study, we provide in vivo evidence showing that *snph* KO sciatic nerves display enhanced regenerative capacity (Fig. 7). This enhanced regeneration is consistent with robustly enhanced mitochondrial motility along *snph* KO sciatic nerves (71.58 ± 2.72%, P < 0.0001) relative to those from WT adult mice (30.948 ± 2.17%; Videos 1 and 2). We also found that GAP-43 expression in *snph* KO DRGs is increased to a larger extent after injury (Fig. 8, A and B). It is well documented that elevated GAP-43 expression is associated with nerve regeneration, potentially recapitulating an early developmental program (Fu and Gordon, 1997; Ackermann et al., 2002; Abe et al., 2010). Alternatively, enhanced mitochondrial transport in mature *snph* KO neurons activates the

early intrinsic program to support neuron regrowth. Exploring how an enhanced energy supply in injured axons impacts the GAP-43 signaling pathway is of great interest in future research.

Our study provides mechanistic insights into how mitochondrial anchoring and energy deficits influence axonal regenerative capacity. Our model is supported by several studies manipulating mitochondrial transport in axons. In the *Caenorhabditis elegans* mutant ric-7, in which mitochondria fail to transport to distal axons, injured axons degenerate rapidly; such degeneration can be suppressed by forcing mitochondria into the axons (Rawson et al., 2014). In an adult fly model, Fang et al. (2012) revealed that axonal mitochondria are rapidly depleted upon axotomy. The injury-induced mitochondrial loss is suppressed by up-regulation of Nmnat, which is known to suppress axon degeneration (Gilley and Coleman, 2010). Interestingly, when mitochondria are genetically eliminated from axons by depleting the kinesin adaptor Milton, up-regulation of Nmnat is no longer effective to suppress axon degeneration (Fang et al., 2012). Similarly, WldS (slow Wallerian degeneration) is an effective protein that suppresses Wallerian degeneration after axon injury (Conforti et al., 2000; Coleman and Freeman, 2010). Using both *Drosophila melanogaster* and mouse models, Avery et al. (2012) identified axonal mitochondria as a key site of action for WldS neuroprotective function. Altogether, these studies consistently suggest that regulating mitochondrial transport is a common target for the signaling pathways protecting injured axons from degeneration.

In summary, our study addresses three fundamental issues as to whether (a) axonal mitochondrial transport is essential for mature neurons to regenerate, (b) enhancing mitochondrial transport facilitates axonal regenerative capacity both in vitro and in vivo, and (c) enhanced mitochondrial transport rescues local energy deficits in injured axons. Our study highlights that reduced mitochondrial transport in mature neurons and injury-induced energy deficits reflect common factors limiting regenerative ca-

pacity. Our in vivo and in vitro experiments suggest that activating an intrinsic "growth program" requires the coordinated modulation of mitochondrial transport and recovery of energy deficits. Such combined approaches may represent a valid therapeutic strategy to facilitate regeneration in the injured CNS and PNS.

Materials and methods

Mouse lines and animal care
The $snph^{-/-}$ mouse line was generated by targeted gene replacement in embryonic stem cells as previously described (Kang et al., 2008). Thy1/Mito-CFP transgenic mice were purchased from the Jackson Laboratory. The mice and the Sprague-Dawley rats were maintained in the National Institute of Neurological Disorders and Stroke (NINDS) animal facility and housed in a 12-h light/dark cycle. All animal procedures were performed according to National Institutes of Health (NIH) guidelines and were approved by the NINDS/National Institute on Deafness and Other Communication Disorders (NIDCD) Animal Care and Use Committee.

Antibodies
The purified polyclonal antibody against SNPH residues 225–428 was described previously (Kang et al., 2008). Sources of other antibodies or reagents are as follows: anti–βIII-tubulin, anti-MAP2, anti-Tau-1, anti-dynein IC74, and anti–GAP-43 were from EMD Millipore; anti–cytochrome c was from BD; anti-TOM20 was from Santa Cruz Biotechnology, Inc.; anti-Miro1/2 (HPA010687) and anti-Trak2 were from Sigma-Aldrich; ECL-HRP–linked secondary antibodies were from GE Healthcare; and Alexa Fluor 546– or Alexa Fluor 488–conjugated secondary antibodies were from Invitrogen.

Lentivirus infection
The cDNA gene encoding SNPH, SNPH-dMTB, or Miro1 was cloned into the lenti-vector pHUGW with the CMV promoter and HA tag; the YFP, GFP-Mito, or PercevalHR (Addgene) and GO-ATeam2 and GO-ATeam3 (gifts from H. Imamura, Kyoto University, Kyoto, Japan) were cloned into pFUGW vector. All lenti-vectors were prepared and transduced at the same concentration. For infection, 2×10^5 freshly dissociated neurons were incubated with up to 5 µl concentrated virus preparation in 25 µl culture medium for 1 h; 200 µl culture media was then added to each side of the wells.

Microfluidic neuron culture and axotomy
For axotomy and staining, both commercialized (#RD450; Xona) and house-made microfluidic devices were used. For the latter, a silicon wafer with a pattern made out of SU-8 by photolithography was used to cast the PDMS microfluidic devices. In brief, SYLGARD 184 silicone elastomer base was mixed with the curing agent at a ratio of 10:1. The PDMS was then mixed well using a THINKY mixer ARF-310 in two steps: mixing at 2,000 rpm for 4 min and de-foaming at 2,200 rpm for 4 min. The well-mixed PDMS was poured onto the silicon wafer and then placed in a Bel-Art vacuum desiccator for 3 h to help remove air bubbles from the PDMS. The wafer with PDMS was placed in an 80°C oven for 1–2 h to cure. Once the PDMS was cured, the PDMS was pulled out, and reservoirs were punched out. The PDMS devices were extensively washed and autoclaved before use. The coverslips and house-made devices were exposed to the plasma treatment for 2 min in a PDC-32G plasma cleaner and bonded together for neuronal culture.

Brain tissues were dissected out from E18–19 mouse embryos and kept in ice-cold Hibernate buffer supplemented with 2% B27 and antibiotics. After the embryos were genotyped by direct tail PCR, cor-

tical neuron cultures were prepared with papain as described previously (Kang et al., 2008). After preparing a single-cell suspension, $2 \times 10^5/20$ µl dissociated neurons were added into the cell body chamber of the microfluidic devices. After cells were attached, 100 µl of prebalanced culture medium was added into each well of the device. Axons pass through microgrooves into the axonal terminal chamber at DIV4 as they grow. For axon regrowth assays, axons in terminal chambers were axotomized by vacuum aspiration at DIV5–7 or DIV12. The two wells on the axon sides were subjected twice to aspiration to ensure complete axotomy. After the first aspiration, Hibernate medium was added to the axon chambers, followed by the second aspiration. The devices were then refilled with fresh culture medium for further incubation for various times, as indicated.

For quantitative analysis of axon growth before and after axotomy, axons in the terminal chamber labeled by lenti-YFP or by βIII-tubulin staining, were imaged under the same setting using an 880 confocal microscope (ZEISS) with a 20× objective. The area of YFP or βIII-tubulin signals above the same threshold within a 1024 × 1024 image that covers all axon segments extending from microgrooves was measured using ImageJ (NIH). Images were collected from multiple chambers in at least three experiments for quantitative analysis.

Adult DRG neuron cultures and Sholl analysis
Adult WT and SNPH KO littermates at P60 were dissected in HBSS. After clipping off bones from the spinal cords, DRGs were pulled out and the excess roots were trimmed off in the HBSS buffer. DRGs were digested in 2.5 U/ml dispase II (Roche) and 200 U/ml collagenase (Worthington Biochemical) for 30 min at 37°C and then an additional 35 min at 30°C. DRG neurons were collected and triturated in Neurobasal-A medium supplemented with B27 and 0.5 mM GlutaMAX (Invitrogen). After purification with 1% BSA cushions, the isolated DRG neuronal cell bodies were plated onto coverslips coated with 30 µg/ml poly-L-ornithine and 5 µg/ml laminin (Roche) at a final density of 2,000 cells per 12-mm coverslip. After 1-d culture in vitro, DRG neurons were stained for imaging, and a Sholl analysis of total numbers of axon intersections was performed with an ImageJ plugin.

Time-lapse imaging and kymograph analysis
To image mitochondrial transport in axons, neurons grown on the PDMS device were replaced with prewarmed Hibernate A low fluorescence medium (BrainBits) supplemented with 2% B27, 0.5 mM GlutaMAX, and 1% Pen/Strep at day of image. The temperature was maintained at 37°C during time-lapse imaging. The microgrooves of the device that contain the fasciculated axon bundles were visualized. Time-lapse imaging of the microgrooves was recorded using a confocal microscope (LSM 510 META; ZEISS) with a C-Apochromat 40×/1.3 oil NA objective (ZEISS). The image sequences were collected at a 512 × 512–pixel resolution (12 bit) with 5-s intervals at a scanning zoom of 1.0 in the x and y directions; 100–200 frames were captured for each condition. For mitochondrial transport before and after axotomy, only 30 frames were recorded to coherently match the time window. To quantify motility, a kymograph was generated by ImageJ as previously described (Kang et al., 2008). For each experimental group, all visible vesicles on the kymograph were pooled together. The mitochondria were considered stationary if they remained immobile during the entire recording period; a mobile one was counted if the net displacement was >5 µm.

Microscope image acquisition
For imaging acquisition, a prescan of all samples was conducted to ensure confocal settings below saturation at 1024 × 1024 pixels (12 bit). From a given experiment, all images were acquired on the same

day with new pinhole adjustment and under the same confocal settings. Morphometric measurements were performed using ImageJ. For ATP/ADP ratio analysis, the neurons transfected with PercevalHR were excited using 488/458 filters, and the emissions were collected at 505–550 nm. For axonal ATP analysis, two emission images were collected at 505–550 nm and long pass above 545 nm along the GO-ATeam2 or GO-ATeam3 expression axon. Radiometric images were generated by an ImageJ macro using binary Mask image to remove nonspecific background in the microgrooves. To analyze axon regrowth, a fixed threshold was manually set to ensure that most signals were detected but not oversaturated with a minimum detectable background. Both the pixel area and fluorescence integrated intensity were measured. For active growth cone quantification, the axon tips that were labeled with 543 phalloidin and βIII-tubulin were imaged and a fixed threshold and particle size were applied for ImageJ analysis. Other parameters are described in the figure legends.

Measurement of mitochondria membrane potential ($\Delta\psi_m$)

Lenti-GFP-Mito was introduced into cultured neurons to label total mitochondria. Before and right after axotomy, nonplasma-treated devices were removed and the exposed axon bundles along microgrooves were loaded with 25 nM TMRE (Invitrogen) for 30 min and then washed three times with B27/Hibernate A low fluorescence medium before imaging. $\Delta\psi_m$ was assessed by relative TMRE fluorescent intensity of each individual mitochondrion labeled by GFP-Mito along the most distal 200 μm of axon bundles on microgrooves using ImageJ particle analysis.

ATP rescue experiments

Neurons were electroporated by Nucleofector (Amaxa) using program O-004 with an electroporation buffer (86 mM KH_2PO_4, 17.5 mM $NaHCO_3$, 2.72 mM D-glucose, and 11.6 mM $MgCl_2$-$6H_2O$) containing 7.1 mM ATP disodium, followed by spin down and removal of the supernatant containing ATP. For ATP rescue study, the electroporated neurons were immediately plated onto a microfluidic chamber with medium containing the final ATP concentration adjusted to 200 μM.

Acquisition of axotomy time-lapse imaging

The multi-timer macro was applied for a combination of laser-based axotomy and time-lapse imaging, as previously described (Yanik et al., 2004; Cho et al., 2013) with some modifications. For axotomy, an LSM 510 META two-photon confocal microscope (ZEISS) with an inverted P-Apochromat 40×/1.3 oil objective was applied. After alignment of scan head and collimator adjustment, Mira 900F laser power was set on to initiate mode-lock without CW break. The stable mode-lock was achieved by tuning the slits on the Coherent Mira 900F. Once the arbitrary units in the power indicator were above 260, the beam wavelength was set to 730 nm for bleaching. For consecutive real-time imaging capture of TMRE and GFP-Mito before and after axotomy, both acquisition and bleach parameters were preset and reloaded in multi-timer macro blocks. In brief, the images in the first block were first recorded at 5-s intervals for a total of 50 frames by 400/543-nm laser in line switch model; then, the second block reloaded the 730-nm laser that powered-up with 70% output and pixel dwell time >10 μs in cropped imaging region for bleaching. The post-axotomy recording was collected at 5-s intervals for a total of 50 or 100 frames by 488/543-nm laser in the final block.

To measure the Ca^{2+} buffering capacity in the adult DRG axons, the neurons were electroporated with green fluorescent Ca^{2+} sensor G-GECO1.2. The same multi-timer macro was applied for consecutive laser axotomy and image acquiring. In brief, after 2 frames of base line acquisition and two-photo laser, 730 nm was applied at the third frame, and then another 26 frames were collected at 512 × 512–pixel resolu-

tion (12 bit) with 3-s intervals. The average decay time constant was calculated based on florescence intensity (F/F_0) curve with nonlinear fit.

For physical axotomy and time-lapse imaging, the pure axon bundle was first stained by TMRE and MitoTracker Green, and images were acquired before and after physical axotomy by using pulled glass capillaries (World Precision Instruments) with a tip diameter of ~1 μm that were prepared from Sutter Instrument (p-97).

In vivo axonal regeneration after injury

For in vivo sciatic nerve injury and axonal regeneration, adult *snph* KO and WT littermates (2 mo old) were subjected to unilateral sciatic nerve crush as described previously (Abe et al., 2010). In brief, under deep anesthesia, the left sciatic nerve was exposed at the mid-thigh level; the nerve was then crushed using fine hemostatic forceps three times, 15 s each time. The wound was sutured in layers, and the mice were allowed to recover on a heating pad. 3 d after injury, mice were perfused transcardially with PBS (pH 7.4) followed by ice-cold 4% PFA in PBS. Sciatic nerves and L4/L5 DRGs from the injured side as well as the contralateral uninjured side were dissected, post-fixed in 4% PFA in PBS for 2 h, and then cryoprotected overnight in 30% sucrose. Specimens were embedded in tissue-freezing medium and then cut longitudinally into serial sections at a thickness of 12 μm. Immunohistochemistry was performed to evaluate axonal regeneration with a GAP-43 antibody to label regenerating axons. Sciatic nerve sections were first blocked with 10% normal goat serum in PBS containing 0.3% Triton X-100 and then incubated with primary antibodies for 1 h at room temperature. The following primary antibodies were used: rabbit anti–GAP-43 antibody (1:800; Abcam), mouse anti–βIII-tubulin antibody (1:1,000; Sigma-Aldrich), or rabbit anti-SNPH antibody (1:400). Sections were washed with PBS, followed by incubation with Alexa Flour 546–conjugated goat anti–rabbit IgG or Alexa Flour 488–conjugated goat anti–mouse IgG (1:500; Invitrogen) secondary antibodies together with DAPI (1:1,000) to visualize nuclei. Slices were mounted and images were acquired using an LSM 880 confocal microscope (ZEISS) with a 20× objective. Three sections spaced 60 μm apart for each sciatic nerve were used to assess axonal regeneration. The nerve was divided into 0.5-mm segments; the number of axons in the segment 0.5 mm proximal to the injury site (0 mm) and in the distal 0.5-, 1.0-, 1.5-, 2.0-, 2.5-, 3.0-, and 3.5-mm segments were quantified and normalized to the number in the injury site.

To examine GAP-43 expression in DRG neuronal cell bodies in response to sciatic nerve injury, 9-wk-old *snph* KO and their WT littermates were subjected to unilateral sciatic nerve crush injury. DRG sections (three sections each) from ipsilateral and contralateral sides of both WT and *snph* KO mice were co-immunostained with antibodies against GAP-43, βIII-tubulin, and DAPI 3 d after sciatic nerve crush injury. Images were obtained using an LSM 880 confocal microscope with a 40× objective. The mean intensity of GAP-43 in individual DRG neuronal cell bodies was measured using ImageJ and normalized to the mean intensity of that from the contralateral uninjured side of WT mice.

Statistical analysis

Statistical analysis was performed using Prism (GraphPad Software). Two groups were compared using F-test, Mann–Whitney (sample size $n < 30$), or Student's t test (sample size $n \geq 30$). For multiple comarisons, one-way ANOVA analysis ($n \geq 30$) or Kruskal–Wallis test ($n < 30$) is used. Data are expressed as mean ± SEM. Differences were considered significant with $P < 0.05$.

Online supplemental material

Fig. S1 shows that deleting *snph* did not change early axonal growth and Miro1/2 expression is not regulated by SNPH. Fig. S2 shows

that enhanced axonal regrowth in *snph* KO neurons is not directly correlated with cell density in the somatic chambers. Fig. S3 shows that overexpressing SNPH alters mitochondrial distribution and ATP/ADP ratios in distal axons. Fig. S4 shows that axotomy stress induces mitochondrial depolarization. Fig. S5 shows energy deficit recovery and calcium buffering in *snph* KO neurons after axotomy. Videos 1 and 2 show ex vivo imaging of axonal mitochondrial transport along sciatic nerves in Thy1-Mito-CFP and in the crossed *snph* KO/Thy1-Mito-CFP mice, respectively. Videos 3–5 show axonal mitochondrial motility along microgrooves from cortical neurons overexpressing SNPH, SNPH-dMTB, or Miro1, respectively. Videos 6 and 7 show axotomy stress depolarizing mitochondria in the vicinity of injured sites. Video 8 shows axonal mitochondrial motility along microgrooves from WT cortical neurons 1 h after axotomy. Video 9 shows enhanced mitochondrial motility along microgrooves from *snph* KO cortical neurons 1 h after axotomy. Online supplemental material is available at http://www.jcb.org/cgi/content/full/jcb.201605101/DC1.

References

Abe, N., and V. Cavalli. 2008. Nerve injury signaling. *Curr. Opin. Neurobiol.* 18:276–283. http://dx.doi.org/10.1016/j.conb.2008.06.005

Abe, N., S.H. Borson, M.J. Gambello, F. Wang, and V. Cavalli. 2010. Mammalian target of rapamycin (mTOR) activation increases axonal growth capacity of injured peripheral nerves. *J. Biol. Chem.* 285:28034–28043. http://dx.doi.org/10.1074/jbc.M110.125336

Ackermann, P.W., M. Ahmed, and A. Kreicbergs. 2002. Early nerve regeneration after achilles tendon rupture—a prerequisite for healing? A study in the rat. *J. Orthop. Res.* 20:849–856. http://dx.doi.org/10.1016/S0736-0266(01)00159-0

Afshari, F.T., S. Kappagantula, and J.W. Fawcett. 2009. Extrinsic and intrinsic factors controlling axonal regeneration after spinal cord injury. *Expert Rev. Mol. Med.* 11:e37. http://dx.doi.org/10.1017/S1462399409001288

Alvarez, S., M. Moldovan, and C. Krarup. 2008. Acute energy restriction triggers Wallerian degeneration in mouse. *Exp. Neurol.* 212:166–178. http://dx.doi.org/10.1016/j.expneurol.2008.03.022

Avery, M.A., T.M. Rooney, J.D. Pandya, T.M. Wishart, T.H. Gillingwater, J.W. Geddes, P.G. Sullivan, and M.R. Freeman. 2012. Wld^S prevents axon degeneration through increased mitochondrial flux and enhanced mitochondrial Ca^{2+} buffering. *Curr. Biol.* 22:596–600. http://dx.doi.org/10.1016/j.cub.2012.02.043

Berg, J., Y.P. Hung, and G. Yellen. 2009. A genetically encoded fluorescent reporter of ATP:ADP ratio. *Nat. Methods.* 6:161–166. http://dx.doi.org/10.1038/nmeth.1288

Bradke, F., J.W. Fawcett, and M.E. Spira. 2012. Assembly of a new growth cone after axotomy: the precursor to axon regeneration. *Nat. Rev. Neurosci.* 13:183–193. http://dx.doi.org/10.1038/nrn3176

Cai, Q., H.M. Zakaria, A. Simone, and Z.H. Sheng. 2012. Spatial parkin translocation and degradation of damaged mitochondria via mitophagy in live cortical neurons. *Curr. Biol.* 22:545–552. http://dx.doi.org/10.1016/j.cub.2012.02.005

Case, L.C., and M. Tessier-Lavigne. 2005. Regeneration of the adult central nervous system. *Curr. Biol.* 15:R749–R753. http://dx.doi.org/10.1016/j.cub.2005.09.008

Cavallucci, V., E. Bisicchia, M.T. Cencioni, A. Ferri, L. Latini, A. Nobili, F. Biamonte, F. Nazio, F. Fanelli, S. Moreno, et al. 2014. Acute focal brain damage alters mitochondrial dynamics and autophagy in axotomized neurons. *Cell Death Dis.* 5:e1545. http://dx.doi.org/10.1038/cddis.2014.511

Chandran, V., G. Coppola, H. Nawabi, T. Omura, R. Versano, E.A. Huebner, A. Zhang, M. Costigan, A. Yekkirala, L. Barrett, et al. 2016. A systems-level analysis of the peripheral nerve intrinsic axonal growth program. *Neuron.* 89:956–970. http://dx.doi.org/10.1016/j.neuron.2016.01.034

Chang, D.T., and I.J. Reynolds. 2006. Mitochondrial trafficking and morphology in healthy and injured neurons. *Prog. Neurobiol.* 80:241–268. http://dx.doi.org/10.1016/j.pneurobio.2006.09.003

Chen, H., and D.C. Chan. 2009. Mitochondrial dynamics—fusion, fission, movement, and mitophagy—in neurodegenerative diseases. *Hum. Mol. Genet.* 18:R169–R176. http://dx.doi.org/10.1093/hmg/ddp326

Chen, Y., and Z.H. Sheng. 2013. Kinesin-1—syntaphilin coupling mediates activity-dependent regulation of axonal mitochondrial transport. *J. Cell Biol.* 202:351–364. http://dx.doi.org/10.1083/jcb.201302040

Cho, Y., and V. Cavalli. 2014. HDAC signaling in neuronal development and axon regeneration. *Curr. Opin. Neurobiol.* 27:118–126. http://dx.doi.org/10.1016/j.conb.2014.03.008

Cho, Y., R. Sloutsky, K.M. Naegle, and V. Cavalli. 2013. Injury-induced HDAC5 nuclear export is essential for axon regeneration. *Cell.* 155:894–908. (published erratum appears in *Cell.* 2015. 161:691) http://dx.doi.org/10.1016/j.cell.2013.10.004

Coleman, M.P., and M.R. Freeman. 2010. Wallerian degeneration, wld(s), and nmnat. *Annu. Rev. Neurosci.* 33:245–267. http://dx.doi.org/10.1146/annurev-neuro-060909-153248

Conforti, L., A. Tarlton, T.G. Mack, W. Mi, E.A. Buckmaster, D. Wagner, V.H. Perry, and M.P. Coleman. 2000. A Ufd2/D4Cole1e chimeric protein and overexpression of Rbp7 in the slow Wallerian degeneration (WldS) mouse. *Proc. Natl. Acad. Sci. USA.* 97:11377–11382. http://dx.doi.org/10.1073/pnas.97.21.11377

Courchet, J., T.L. Lewis Jr., S. Lee, V. Courchet, D.Y. Liou, S. Aizawa, and F. Polleux. 2013. Terminal axon branching is regulated by the LKB1-NUAK1 kinase pathway via presynaptic mitochondrial capture. *Cell.* 153:1510–1525. http://dx.doi.org/10.1016/j.cell.2013.05.021

Court, F.A., and M.P. Coleman. 2012. Mitochondria as a central sensor for axonal degenerative stimuli. *Trends Neurosci.* 35:364–372. http://dx.doi.org/10.1016/j.tins.2012.04.001

Das, S., J. Boczan, C. Gerwin, P.B. Zald, and Z.H. Sheng. 2003. Regional and developmental regulation of syntaphilin expression in the brain: a candidate molecular element of synaptic functional differentiation. *Brain Res. Mol. Brain Res.* 116:38–49. http://dx.doi.org/10.1016/S0169-328X(03)00212-2

Di Giovanni, J., and Z.H. Sheng. 2015. Regulation of synaptic activity by snapin-mediated endolysosomal transport and sorting. *EMBO J.* 34:2059–2077. http://dx.doi.org/10.15252/embj.201591125

Fang, Y., L. Soares, X. Teng, M. Geary, and N.M. Bonini. 2012. A novel *Drosophila* model of nerve injury reveals an essential role of Nmnat in maintaining axonal integrity. *Curr. Biol.* 22:590–595. http://dx.doi.org/10.1016/j.cub.2012.01.065

Filbin, M.T. 2006. Recapitulate development to promote axonal regeneration: good or bad approach? *Philos. Trans. R. Soc. Lond. B Biol. Sci.* 361:1565–1574. http://dx.doi.org/10.1098/rstb.2006.1885

Fitch, M.T., and J. Silver. 2008. CNS injury, glial scars, and inflammation: Inhibitory extracellular matrices and regeneration failure. *Exp. Neurol.* 209:294–301. http://dx.doi.org/10.1016/j.expneurol.2007.05.014

Fu, S.Y., and T. Gordon. 1997. The cellular and molecular basis of peripheral nerve regeneration. *Mol. Neurobiol.* 14:67–116. http://dx.doi.org/10.1007/BF02740621

Giger, R.J., E.R. Hollis II, and M.H. Tuszynski. 2010. Guidance molecules in axon regeneration. *Cold Spring Harb. Perspect. Biol.* 2:a001867. http://dx.doi.org/10.1101/cshperspect.a001867

Gilley, J., and M.P. Coleman. 2010. Endogenous Nmnat2 is an essential survival factor for maintenance of healthy axons. *PLoS Biol.* 8:e1000300. http://dx.doi.org/10.1371/journal.pbio.1000300

Goslin, K., D.J. Schreyer, J.H. Skene, and G. Banker. 1988. Development of neuronal polarity: GAP-43 distinguishes axonal from dendritic growth cones. *Nature.* 336:672–674. http://dx.doi.org/10.1038/336672a0

Harel, N.Y., and S.M. Strittmatter. 2006. Can regenerating axons recapitulate developmental guidance during recovery from spinal cord injury? *Nat. Rev. Neurosci.* 7:603–616. http://dx.doi.org/10.1038/nrn1957

Hill, C.E., M.S. Beattie, and J.C. Bresnahan. 2001. Degeneration and sprouting of identified descending supraspinal axons after contusive spinal cord injury in the rat. *Exp. Neurol.* 171:153–169. http://dx.doi.org/10.1006/exnr.2001.7734

Hoffman, P.N. 2010. A conditioning lesion induces changes in gene expression and axonal transport that enhance regeneration by increasing the intrinsic growth state of axons. *Exp. Neurol.* 223:11–18. http://dx.doi.org/10.1016/j.expneurol.2009.09.006

Hu, Y., K.K. Park, L. Yang, X. Wei, Q. Yang, K.S. Cho, P. Thielen, A.H. Lee, R. Cartoni, L.H. Glimcher, et al. 2012. Differential effects of unfolded protein response pathways on axon injury-induced death of retinal ganglion cells. *Neuron.* 73:445–452. http://dx.doi.org/10.1016/j.neuron.2011.11.026

Kang, J.S., J.H. Tian, P.Y. Pan, P. Zald, C. Li, C. Deng, and Z.H. Sheng. 2008. Docking of axonal mitochondria by syntaphilin controls their mobility and affects short-term facilitation. *Cell.* 132:137–148. http://dx.doi.org/10.1016/j.cell.2007.11.024

Koeberle, P.D., and A.K. Ball. 1999. Nitric oxide synthase inhibition delays axonal degeneration and promotes the survival of axotomized retinal ganglion cells. *Exp. Neurol.* 158:366–381. http://dx.doi.org/10.1006/exnr.1999.7113

Li, Y., and G. Raisman. 1995. Sprouts from cut corticospinal axons persist in the presence of astrocytic scarring in long-term lesions of the adult rat spinal cord. *Exp. Neurol.* 134:102–111. http://dx.doi.org/10.1006/exnr.1995.1041

Liu, K., A. Tedeschi, K.K. Park, and Z. He. 2011. Neuronal intrinsic mechanisms of axon regeneration. *Annu. Rev. Neurosci.* 34:131–152. http://dx.doi.org/10.1146/annurev-neuro-061010-113723

Lucius, R., and J. Sievers. 1996. Postnatal retinal ganglion cells in vitro: protection against reactive oxygen species (ROS)-induced axonal degeneration by cocultured astrocytes. *Brain Res.* 743:56–62. http://dx.doi.org/10.1016/S0006-8993(96)01029-3

MacAskill, A.F., and J.T. Kittler. 2010. Control of mitochondrial transport and localization in neurons. *Trends Cell Biol.* 20:102–112. http://dx.doi.org/10.1016/j.tcb.2009.11.002

Miller, K.E., and M.P. Sheetz. 2004. Axonal mitochondrial transport and potential are correlated. *J. Cell Sci.* 117:2791–2804. http://dx.doi.org/10.1242/jcs.01130

Misgeld, T., M. Kerschensteiner, F.M. Bareyre, R.W. Burgess, and J.W. Lichtman. 2007. Imaging axonal transport of mitochondria in vivo. *Nat. Methods.* 4:559–561. http://dx.doi.org/10.1038/nmeth1055

Morris, R.L., and P.J. Hollenbeck. 1993. The regulation of bidirectional mitochondrial transport is coordinated with axonal outgrowth. *J. Cell Sci.* 104:917–927.

Nakano, M., H. Imamura, T. Nagai, and H. Noji. 2011. Ca^{2+} regulation of mitochondrial ATP synthesis visualized at the single cell level. *ACS Chem. Biol.* 6:709–715. http://dx.doi.org/10.1021/cb100313n

Nicholls, D.G., and S.L. Budd. 2000. Mitochondria and neuronal survival. *Physiol. Rev.* 80:315–360.

O'Donnell, K.C., M.E. Vargas, and A. Sagasti. 2013. WldS and PGC-1α regulate mitochondrial transport and oxidation state after axonal injury. *J. Neurosci.* 33:14778–14790. http://dx.doi.org/10.1523/JNEUROSCI.1331-13.2013

Park, K.K., K. Liu, Y. Hu, P.D. Smith, C. Wang, B. Cai, B. Xu, L. Connolly, I. Kramvis, M. Sahin, and Z. He. 2008. Promoting axon regeneration in the adult CNS by modulation of the PTEN/mTOR pathway. *Science.* 322:963–966. http://dx.doi.org/10.1126/science.1161566

Perlson, E., G.B. Jeong, J.L. Ross, R. Dixit, K.E. Wallace, R.G. Kalb, and E.L. Holzbaur. 2009. A switch in retrograde signaling from survival to stress in rapid-onset neurodegeneration. *J. Neurosci.* 29:9903–9917. http://dx.doi.org/10.1523/JNEUROSCI.0813-09.2009

Rawson, R.L., L. Yam, R.M. Weimer, E.G. Bend, E. Hartwieg, H.R. Horvitz, S.G. Clark, and E.M. Jorgensen. 2014. Axons degenerate in the absence of mitochondria in *C. elegans*. *Curr. Biol.* 24:760–765. http://dx.doi.org/10.1016/j.cub.2014.02.025

Ruthel, G., and P.J. Hollenbeck. 2003. Response of mitochondrial traffic to axon determination and differential branch growth. *J. Neurosci.* 23:8618–8624.

Saxton, W.M., and P.J. Hollenbeck. 2012. The axonal transport of mitochondria. *J. Cell Sci.* 125:2095–2104. http://dx.doi.org/10.1242/jcs.053850

Schwab, M.E., and D. Bartholdi. 1996. Degeneration and regeneration of axons in the lesioned spinal cord. *Physiol. Rev.* 76:319–370.

Sheng, Z.H. 2014. Mitochondrial trafficking and anchoring in neurons: New insight and implications. *J. Cell Biol.* 204:1087–1098. http://dx.doi.org/10.1083/jcb.201312123

Sheng, Z.H., and Q. Cai. 2012. Mitochondrial transport in neurons: impact on synaptic homeostasis and neurodegeneration. *Nat. Rev. Neurosci.* 13:77–93. http://dx.doi.org/10.1038/nrn3156

Spillane, M., A. Ketschek, T.T. Merianda, J.L. Twiss, and G. Gallo. 2013. Mitochondria coordinate sites of axon branching through localized intra-axonal protein synthesis. *Cell Reports.* 5:1564–1575. http://dx.doi.org/10.1016/j.celrep.2013.11.022

Sun, F., K.K. Park, S. Belin, D. Wang, T. Lu, G. Chen, K. Zhang, C. Yeung, G. Feng, B.A. Yankner, and Z. He. 2011. Sustained axon regeneration induced by co-deletion of PTEN and SOCS3. *Nature.* 480:372–375. http://dx.doi.org/10.1038/nature10594

Sun, T., H. Qiao, P.Y. Pan, Y. Chen, and Z.H. Sheng. 2013. Motile axonal mitochondria contribute to the variability of presynaptic strength. *Cell Reports.* 4:413–419. http://dx.doi.org/10.1016/j.celrep.2013.06.040

Tantama, M., J.R. Martínez-François, R. Mongeon, and G. Yellen. 2013. Imaging energy status in live cells with a fluorescent biosensor of the intracellular ATP-to-ADP ratio. *Nat. Commun.* 4:2550. http://dx.doi.org/10.1038/ncomms3550

Tao, K., N. Matsuki, and R. Koyama. 2014. AMP-activated protein kinase mediates activity-dependent axon branching by recruiting mitochondria to axon. *Dev. Neurobiol.* 74:557–573. http://dx.doi.org/10.1002/dneu.22149

Tessier-Lavigne, M., and C.S. Goodman. 1996. The molecular biology of axon guidance. *Science.* 274:1123–1133. http://dx.doi.org/10.1126/science.274.5290.1123

Yanik, M.F., H. Cinar, H.N. Cinar, A.D. Chisholm, Y. Jin, and A. Ben-Yakar. 2004. Neurosurgery: functional regeneration after laser axotomy. *Nature.* 432:822. http://dx.doi.org/10.1038/432822a

Yiu, G., and Z. He. 2006. Glial inhibition of CNS axon regeneration. *Nat. Rev. Neurosci.* 7:617–627. http://dx.doi.org/10.1038/nrn1956

Yu, T.W., and C.I. Bargmann. 2001. Dynamic regulation of axon guidance. *Nat. Neurosci.* 4:1169–1176. http://dx.doi.org/10.1038/nn748

Zhao, Y., S. Araki, J. Wu, T. Teramoto, Y.F. Chang, M. Nakano, A.S. Abdelfattah, M. Fujiwara, T. Ishihara, T. Nagai, and R.E. Campbell. 2011. An expanded palette of genetically encoded Ca^{2+} indicators. *Science.* 333:1888–1891. http://dx.doi.org/10.1126/science.1208592

Zhou, B., Q. Cai, Y. Xie, and Z.H. Sheng. 2012. Snapin recruits dynein to BDNF-TrkB signaling endosomes for retrograde axonal transport and is essential for dendrite growth of cortical neurons. *Cell Reports.* 2:42–51. http://dx.doi.org/10.1016/j.celrep.2012.06.010